Chapter 5 New Physics at the TeV Scale and Beyond

1   Introduction

The impressive amount of data collected in the past several decades in particle physics experiments is well accommodated by the Standard Model. This model provides an accurate description of Nature up to energies of order 100 GeV. Nonetheless, the Standard Model is an incomplete theory, since many key elements are left unexplained: (i) the origin of electroweak symmetry breaking, (ii) the generation and stabilization of the hierarchy, $i.e.$, the large disparity between the electroweak and the Planck scale, (iii) the connection of elementary particle forces with gravity, and (iv) the generation of fermion masses and mixings. These deficiencies imply that there is physics beyond the Standard Model and point toward the principal goal of particle physics during the next decade: the elucidation of the electroweak symmetry breaking mechanism and the new physics that must necessarily accompany it. Electroweak symmetry is broken at the TeV scale. In the absence of highly unnatural fine-tuning of the parameters in the underlying theory, the energy scales of the associated new phenomena should also lie in the TeV range or below.

Numerous theories have been proposed to address these outstanding issues and embed the Standard Model in a larger framework. In this chapter, we demonstrate the ability of a linear collider operating at 500 GeV and above to make fundamental progress in the illumination of new phenomena over the broadest possible range. The essential role played by e^+e^- machines in this endeavor has a strong history. First, e^+e^- colliders are discovery machines and are complementary to hadron colliders operating at similar energy regions. The discoveries of the gluon, charm, and tau sustain this assertion. Here, we show that 500-1000 GeV is a discovery energy region and that e^+e^- experiments there add to the search capability of the LHC in many scenarios. Second, e^+e^- collisions offer excellent tools for the intensive study of new phenomena, to precisely determine the properties of new particles and interactions, and to unravel the underlying theory. This claim is chronicled by the successful program at the Z pole carried out at LEP and the SLC. The diagnostic tests of new physics scenarios provided by a 500–1000 GeV linear collider are detailed in this chapter. For the new physics discovered at the LHC or at the LC, the linear collider will provide further information on what it is and how it relates to higher energy scales.

Chapter 9 of this book gives a survey of the various possible mechanisms for electroweak symmetry breaking that motivate the search for new physics beyond the Standard Model at energies below 1 TeV. Among these models, supersymmetry has

been the most intensively studied in the past few years. We have devoted Chapter 4 of this document to a discussion of how supersymmetry can be studied at a linear collider. But supersymmetry is only one of many proposals that have been made for the nature of the new physics that will appear at the TeV scale. In this chapter, we will discuss how several other classes of models can be tested at the linear collider. We will also discuss the general experimental probes of new physics that the linear collider makes available.

The first few sections of this chapter present the tools that linear collider experiments bring to models in which electroweak symmetry breaking is the result of new strong interactions at the TeV energy scale. We begin this study in Section 2 with a discussion of precision measurements of the W and Z boson couplings. New physics at the TeV scale typically modifies the couplings of the weak gauge bosons, generating, in particular, anomalous contributions to the triple gauge couplings (TGCs). These effects appear both in models with strong interactions in the Higgs sector, where they are essentially nonperturbative, and in models with new particles, including supersymmetry, where they arise as perturbative loop corrections. We document the special power of the linear collider to observe these effects.

In Section 3, we discuss the role of linear collider experiments in studying models in which electroweak symmetry breaking arises from new strong interactions. These include both models with no Higgs boson and models in which the Higgs boson is a composite of more fundamental fermions. The general methods from Section 2 play an important role in this study, but there are also new features specific to each class of model.

In Section 4, we discuss the related notion that quarks and leptons are composite states built of more fundamental constituents. The best tests for composite structure of quarks and leptons involve the sort of precision measurements that are a special strength of the linear collider.

In Section 5, we discuss the ability of linear collider experiments to discover new gauge bosons. New Z and W bosons arise in many extensions of the Standard Model. They may result, for example, from extended gauge groups of grand unification or from new interactions associated with a strongly coupled Higgs sector. The linear collider offers many different experimental probes for these particles, involving their couplings to all Standard Model species that are pair-produced in e^+e^- annihilation. This experimental program neatly complements the capability of the LHC to discover new gauge bosons as resonances in dilepton production. We describe how the LHC and linear collider results can be put together to obtain a complete phenomenological profile of a Z'. Grand unified models that lead to Z' bosons often also lead to exotic fermions, so we also discuss the experiments that probe for these particles at a linear collider.

It is possible that the new physics at the TeV scale includes the appearance of new dimensions of space. In fact, models with extra spatial dimensions have recently been

introduced to address the outstanding problems of the Standard Model, including the origin of electroweak symmetry breaking. In Section 6, we review these models and explain how they can be tested at a linear collider.

Further new and distinctive ideas about physics beyond the Standard Model are likely to appear in the future. We attempt to explore this unchartered territory in Section 7 by discussing collider tests of some unconventional possibilities arising from string theory. More generally, our limited imagination cannot span the whole range of alternatives for new physics allowed by the current data. We must prepare to discover the unexpected!

Finally, we devote Section 8 to a discussion of the determination of the origin of new physics effects. Many investigations of new phenomena at colliders focus only on defining the search reach. But once a discovery is made, the next step is to elucidate the characteristics of the new phenomena. At the linear collider, general methods such as the precision study of W pair production and fermion-antifermion production can give signals in many different scenarios for new physics. However, the specific signals expected in each class of models are characteristic and can be used to distinguish the possibilities. We give an example of this and review the tools that the linear collider provides to distinguish between possible new physics sources.

We shall see in this chapter that the reach of the linear collider to discover new physics and the ability of the linear collider to perform detailed diagnostic tests combine to provide a facility with very strong capabilities to study the unknown new phenomena that we will meet at the next step in energy.

2   Gauge boson self-couplings

The measurement of gauge boson self-couplings at a linear collider can provide insight into new physics processes in the presence or absence of new particle production. In the absence of particle resonances, and in particular in the absence of a Higgs boson resonance, the measurement of gauge boson self-couplings will provide a window to the new physics responsible for electroweak symmetry breaking. If there are many new particles being produced—if, for example, supersymmetric particles abound—then the measurement of gauge boson self-couplings will prove valuable since the gauge boson self-couplings will reflect the properties of the new particles through radiative corrections.

2.1   Triple gauge boson coupling overview

Gauge boson self-couplings include the triple gauge couplings (TGCs) and quartic gauge couplings (QGCs) of the photon, W and Z. Of special importance at a linear collider are the $WW\gamma$ and WWZ TGCs since a large sample of fully reconstructed $e^+e^- \rightarrow W^+W^-$ events will be available to measure these couplings.

The effective Lagrangian for the general W^+W^-V vertex ($V = \gamma, Z$) contains 7 complex TGCs, denoted by g_1^V, κ_V, λ_V, g_4^V, g_5^V, $\tilde{\kappa}_V$, and $\tilde{\lambda}_V$ [1]. The magnetic dipole and electric quadrupole moments of the W are linear combinations of κ_γ and λ_γ while the magnetic quadrupole and electric dipole moments are linear combinations of $\tilde{\kappa}_\gamma$ and $\tilde{\lambda}_\gamma$. The TGCs g_1^V, κ_V, and λ_V are C- and P-conserving, g_5^V is C- and P-violating but conserves CP, and g_4^V, $\tilde{\kappa}_V$, and $\tilde{\lambda}_V$ are CP-violating. In the SM at tree-level all the TGCs are zero except $g_1^V = \kappa_V = 1$.

If there is no Higgs boson resonance below about 800 GeV, the interactions of the W and Z gauge bosons become strong above 1 TeV in the WW, WZ or ZZ center-of-mass system. In analogy with $\pi\pi$ scattering below the ρ resonance, the interactions of the W and Z bosons below the strong symmetry breaking resonances can be described by an effective chiral Lagrangian [2]. These interactions induce anomalous TGC's at tree-level:

$$
\begin{aligned}
\kappa_\gamma &= 1 + \frac{e^2}{32\pi^2 s_w^2}(L_{9L} + L_{9R}) \\
\kappa_Z &= 1 + \frac{e^2}{32\pi^2 s_w^2}\left(L_{9L} - \frac{s_w^2}{c_w^2}L_{9R}\right) \\
g_1^Z &= 1 + \frac{e^2}{32\pi^2 s_w^2}\frac{L_{9L}}{c_w^2} \ ,
\end{aligned}
$$

where $s_w^2 = \sin^2\theta_w$, $c_w^2 = \cos^2\theta_w$, and L_{9L} and L_{9R} are chiral Lagrangian parameters. If we replace L_{9L} and L_{9R} by the values of these parameters in QCD, κ_γ is shifted by $\Delta\kappa_\gamma \sim -3 \times 10^{-3}$.

Standard Model radiative corrections [3] cause shifts in the TGCs of $\mathcal{O}(10^{-4} - 10^{-3})$ for CP-conserving couplings and of $\mathcal{O}(10^{-10} - 10^{-8})$ for CP-violating TGC's. Radiative corrections in the MSSM can cause shifts of $\mathcal{O}(10^{-4} - 10^{-2})$ in both the CP-conserving [4] and CP-violating TGC's [5].

2.2 Triple gauge boson measurements

The methods used at LEP2 to measure TGCs provide a useful guide to the measurement of TGCs at a linear collider. When measuring TGCs the kinematics of an $e^+e^- \to W^+W^-$ event can be conveniently expressed in terms of the W^+W^- center-of-mass energy following initial-state radiation (ISR), the masses of the W^+ and W^-, and five angles: the angle between the W^- and initial e^- in the W^+W^- rest frame, the polar and azimuthal angles of the fermion in the rest frame of its parent W^-, and the polar and azimuthal angles of the anti-fermion in the rest frame of its parent W^+.

In practice not all of these variables can be reconstructed unambiguously. For example, in events with hadronic decays it is often difficult to measure the flavor of the quark jet, and so there is usually a two-fold ambiguity for quark jet directions. Also,

it can be difficult to measure ISR and consequently the measured W^+W^- center-of-mass energy is often just the nominal $\sqrt{s}$. Monte Carlo simulation is used to account for detector resolution, quark hadronization, initial- and final-state radiation, and other effects.

The TGC measurement error at a linear collider can be estimated to a good approximation by considering $e\nu q\bar{q}$ and $\mu\nu q\bar{q}$ channels only, and by ignoring all detector and radiation effects except for the requirement that the W^+W^- fiducial volume be restricted to $|\cos\theta_W| < 0.9$. Such an approach correctly predicts the TGC sensitivity of LEP2 experiments and of detailed linear collider simulations [6]. This rule-of-thumb approximation works because LEP2 experiments and detailed linear collider simulations also use the $\tau\nu q\bar{q}$, $\ell\nu\ell\nu$ and $q\bar{q}q\bar{q}$ channels, and the increased sensitivity from these extra channels makes up for the lost sensitivity due to detector resolution, initial- and final-state radiation, and systematic errors.

Table 5.1 contains the estimates of the TGC precision that can be obtained at $\sqrt{s} = 500$ and 1000 GeV for the CP-conserving couplings g_1^V, κ_V, and λ_V. These estimates are derived from one-parameter fits in which all other TGC parameters are kept fixed at their tree-level SM values. Table 5.2 contains the corresponding estimates for the C- and P-violating couplings $\tilde{\kappa}_V$, $\tilde{\lambda}_V$, g_4^V, and g_5^V. An alternative method of measuring the $WW\gamma$ couplings is provided by the channel $e^+e^- \rightarrow \nu\bar{\nu}\gamma$ [7].

The difference in TGC precision between the LHC and a linear collider depends on the TGC, but typically the TGC precision at the linear collider will be substantially better, even at $\sqrt{s} = 500$ GeV. Figure 5.1 shows the measurement precision expected for the LHC [8] and for linear colliders of three different energies for four different TGCs.

If the goal of a TGC measurement program is to search for the first sign of deviation from the SM, one-parameter fits in which all other TGCs are kept fixed at their tree-level SM values are certainly appropriate. But what if the goal is to survey a large number TGCs, all of which seem to deviate from their SM value? Is a 28-parameter fit required? The answer is probably no, as illustrated in Fig. 5.2.

Figure 5.2 shows the histogram of the correlation coefficients for all 171 pairs of TGCs when 19 different TGCs are measured at LEP2 using one-parameter fits. The entries in Fig. 5.2 with large positive correlations are pairs of TGCs that are related to each other by the interchange of γ and Z. The correlation between the two TGCs of each pair can be removed using the dependence on electron beam polarization. The entries in Fig. 5.2 with large negative correlations are TGC pairs of the type $Re(\tilde{\kappa}_\gamma)/Re(\tilde{\lambda}_\gamma)$, $Re(\tilde{\kappa}_Z)/Re(\tilde{\lambda}_Z)$, *etc.* Half of the TGC pairs with large negative correlations will become uncorrelated once polarized electron beams are used, leaving only a small number of TGC pairs with large negative or positive correlation coefficients.

189
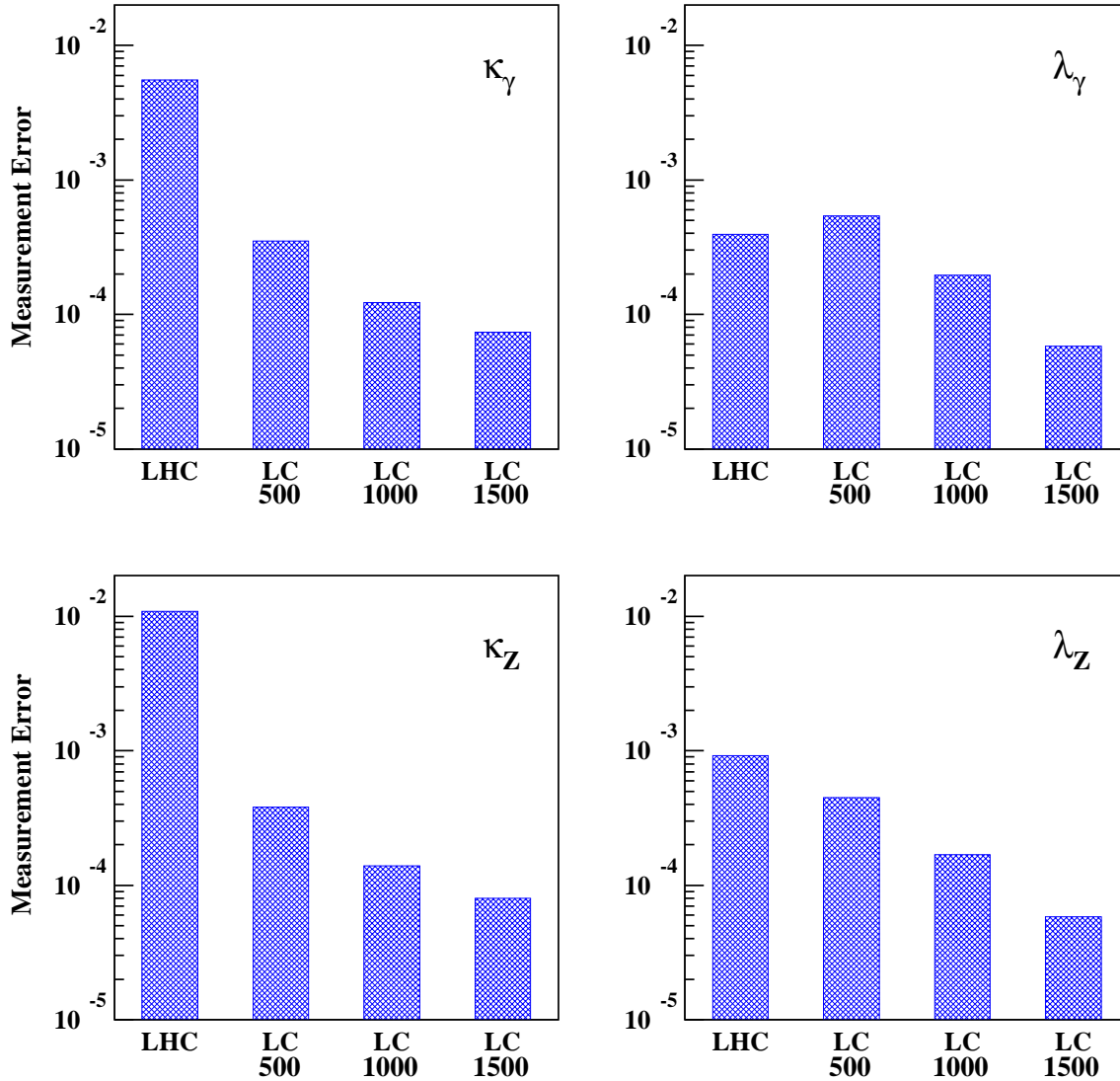
Figure 5.1: Expected measurement error for the real part of four different TGCs. The numbers below the "LC" labels refer to the center-of-mass energy of the linear collider in GeV. The luminosity of the LHC is assumed to be 300 fb^{-1}, while the luminosities of the linear colliders are assumed to be 500, 1000, and 1000 fb^{-1} for $\sqrt{s}$=500, 1000, and 1500 GeV respectively.

	error $\times 10^{-4}$			
	$\sqrt{s} = 500$ GeV		$\sqrt{s} = 1000$ GeV	
TGC	Re	Im	Re	Im
g_1^γ	15.5	18.9	12.8	12.5
κ_γ	3.5	9.8	1.2	4.9
λ_γ	5.4	4.1	2.0	1.4
g_1^Z	14.1	15.6	11.0	10.7
κ_Z	3.8	8.1	1.4	4.2
λ_Z	4.5	3.5	1.7	1.2

Table 5.1: Expected errors for the real and imaginary parts of CP-conserving TGCs assuming $\sqrt{s} = 500$ GeV, $\mathcal{L} = 500$ fb^{-1} and $\sqrt{s} = 1000$ GeV, $\mathcal{L} = 1000$ fb^{-1}. The results are for one-parameter fits in which all other TGCs are kept fixed at their SM values.

	error $\times 10^{-4}$			
	$\sqrt{s} = 500$ GeV		$\sqrt{s} = 1000$ GeV	
TGC	Re	Im	Re	Im
$\tilde{\kappa}_\gamma$	22.5	16.4	14.9	12.0
$\tilde{\lambda}_\gamma$	5.8	4.0	2.0	1.4
$\tilde{\kappa}_Z$	17.3	13.8	11.8	10.3
$\tilde{\lambda}_Z$	4.6	3.4	1.7	1.2
g_4^γ	21.3	18.8	13.9	12.8
g_5^γ	19.3	21.6	13.3	13.4
g_4^Z	17.9	15.2	12.0	10.4
g_5^Z	16.0	16.7	11.4	10.7

Table 5.2: Expected errors for the real and imaginary parts of C- and P-violating TGCs assuming $\sqrt{s} = 500$ GeV, $\mathcal{L} = 500$ fb^{-1} and $\sqrt{s} = 1000$ GeV, $\mathcal{L} = 1000$ fb^{-1}. The results are for one-parameter fits in which all other TGCs are kept fixed at their SM values.

2.3 Electroweak radiative corrections to $e^+e^- \to 4$ fermions

We have seen that the experimental accuracy at a linear collider for the basic electroweak cross section measurements is expected to be at the level of $0.1 - 0.01\%$, requiring the inclusion of electroweak radiative corrections to the predictions for the underlying production processes such as $e^+e^- \to WW \to 4f$.

The full treatment of the processes $e^+e^- \to 4f$ at the one-loop level is of enormous
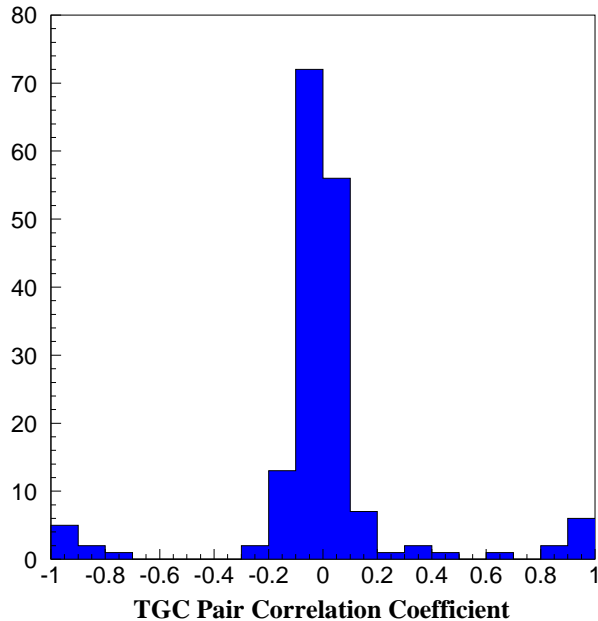
Figure 5.2: Histogram of correlation coefficients for all 171 pairs of TGCs when 19 different TGCs are measured using one-parameter fits at LEP2 (unpolarized beams). The 19 TGCs are made up of the real and imaginary parts of the 8 C- and P-violating couplings along with the real parts of the three CP-conserving couplings g_1^Z, κ_γ, λ_γ.

complexity. Nevertheless there is ongoing work in this direction [9]. While the real bremsstrahlung contribution is known exactly, there are severe theoretical problems with the virtual order-α corrections. A detailed description of the status of predictions for $e^+e^- \to 4f(\gamma)$ processes can be found in [10]. A suitable approach to include order-α corrections to gauge-boson pair production is a double-pole approximation (DPA), keeping only those terms in an expansion about the gauge-boson resonance poles that are enhanced by two resonant gauge bosons. All present calculations of order-α corrections to $e^+e^- \to WW \to 4f$ rely on a DPA [11–14]. Different versions of a DPA have been implemented in the Monte Carlo (MC) generators RacoonWW [12] and YFSWW3 [13]. The intrinsic DPA error is estimated to be $\alpha\Gamma_W/(\pi M_W) \sim 0.5\%$ whenever the cross section is dominated by doubly resonant contributions. This is the case at LEP2 energies sufficiently above threshold. The DPA is not a valid approximation close to the W-pair production threshold. At higher energies diagrams without two resonant W bosons become sizable, especially single W production, and appropriate cuts must be applied to extract the WW signal.

The theoretical uncertainty of present predictions for the total W-pair production

cross section, σ_{WW}, is of the order of 0.5% for energies between 170 GeV and 500 GeV [10], which is within the expected DPA uncertainty. This is a result of a tuned numerical comparison between the state-of-the-art MC generators RacoonWW and YFSWW3, supported by a comparison with a semi-analytical calculation [11] and a study of the intrinsic DPA ambiguity with RacoonWW [10,12]. In the threshold region σ_{WW} is known only to about 2%, since predictions are based on an improved Born approximation [10] that neglects non-universal electroweak corrections. Further improvements of the theoretical uncertainty on σ_{WW} are anticipated only when the full order-α calculation becomes available. Above 500 GeV, large electroweak logarithms of Sudakov type become increasingly important and contributions of higher orders need to be taken into account.

A tuned comparison has also been performed of RacoonWW and YFSWW3 predictions for the W invariant mass and the W production angle distributions, as well as for several photon observables such as photon energy and production angle distributions, at 200 GeV [10,15] and 500 GeV [15]. Taking the observed differences between the RacoonWW and YFSWW3 predictions as a guideline, a theoretical uncertainty of the order of 1% can be assigned to the W production angle distribution and the W invariant mass distribution in the W resonance region. A recent comparison of RacoonWW predictions for photon observables including leading higher-order initial-state radiation [15] with YFSWW3 predictions yields relative differences of less than 5% at 200 GeV and about 10% at 500 GeV. These differences might be attributed to the different treatment of visible photons in the two MC generators: in RacoonWW the real order-α corrections are based on the full $4f + \gamma$ matrix element, while in YFSWW3 multi-photon radiation in W-pair production is combined with order-α^2 LL photon radiation in W decays.

2.4 Quartic gauge boson couplings

The potential for directly probing anomalous quartic gauge boson couplings (AQGCs) via triple gauge-boson production at LEP2, at a future high-energy LC, and at hadron colliders has been investigated in [15–19], [15,16,21–23] and [18,24,25], respectively. The AQGCs under study arise from genuine 4- and 6-dimensional operators, *i.e.*, they have no connection to the parametrization of the anomalous TGCs. It is conceivable that there are extensions of the SM that leave the SM TGCs unchanged but modify quartic self-interactions of the electroweak gauge bosons [21]. The possible number of operators is considerably reduced by imposing a global custodial SU(2) symmetry to protect the ρ parameter from large contributions, *i.e.*, to keep ρ close to 1, and by the local U(1)$_{\text{QED}}$ symmetry whenever a photon is involved.

The sensitivity of triple-gauge-boson cross sections to dimension-4 operators, which only involve massive gauge bosons, has been studied for a high-energy LC and the LHC in [21,23] and [24], respectively. Only weak constraints are expected from WWW, WWZ, WZZ and ZZZ productions at the LHC [24], but these processes

may provide complementary information if non-zero AQGCs are found. The genuine dimension-4 AQGCs may be best probed in a multi-TeV LC. The sensitivity to the two $SU(2)_c$-conserving AQGCs in the processes $e^+e^- \to 6f$ at a 1 TeV LC with a luminosity of 1000 fb^{-1} can be expected to be between 10^{-3} and 10^{-2} [23].

The following discussion is restricted to AQGCs involving at least one photon, which can be probed in $WW\gamma, ZZ\gamma, Z\gamma\gamma$ and $W\gamma\gamma$ production. The lowest-dimension operators that lead to the photonic AQGCs a_0, a_c, a_n, $\tilde{a}_0$, and $\tilde{a}_n$ are of dimension-6 [15,21,22,25] and yield anomalous contributions to the SM $WW\gamma\gamma, WWZ\gamma$ vertices, and a non-standard $ZZ\gamma\gamma$ interaction at the tree level. Most studies of AQGCs consider the separately P- and C-conserving couplings a_0, a_c and the CP-violating coupling a_n. Recently the P-violating AQGCs $\tilde{a}_0$, and $\tilde{a}_n$ have also been considered [15]. More general AQGCs that have been embedded in manifestly $SU(2)_L \times U(1)_Y$ gauge invariant operators are discussed in [17,19]. The AQGCs depend on a mass scale Λ characterizing the scale of new physics. The choice for Λ is arbitrary as long as no underlying model is specified which gives rise to the AQGCs. For instance, anomalous quartic interactions may be interpreted as contact interactions, which might be the manifestation of the exchange of heavy particles with a mass scale Λ.

Recently, at LEP2, the first direct bounds on the AQGCs a_0, a_c, a_n have been imposed by investigating the total cross sections and photon energy distributions for the processes $e^+e^- \to WW\gamma, Z\gamma\gamma, Z\nu\overline{\nu}$ [20]. The results, in units of GeV^{-2}, are

$$-0.037 < \frac{a_0}{\Lambda^2} < 0.036 \qquad -0.077 < \frac{a_c}{\Lambda^2} < 0.095 \qquad -0.45 < \frac{a_n}{\Lambda^2} < 0.41 \,, \quad (5.1)$$

for 95% CL intervals. These limits are expected to improve considerably as the energy increases. It has been found that a 500 GeV LC with a total integrated luminosity of 500 fb^{-1} can improve the LEP2 limits by as much as three orders of magnitude [17].

At hadron colliders the search for AQGCs is complicated by an arbitrary form factor that is introduced to suppress unitarity-violating contributions at large parton center-of-mass energies. At the LHC, however, the dependence of a measurement of AQGCs on the form-factor parametrization may be avoided by measuring energy-dependent AQGCs [24]. At Run II of the Tevatron at 2 TeV, with 2 fb^{-1}, AQGC limits comparable to the LEP2 limits are expected [18,25].

Numerical studies of AQGCs are not yet as sophisticated as the ones for TGCs. For instance, most studies of AQGCs have not yet included gauge boson decays, and MC generators for the process $e^+e^- \to 4f + \gamma$ including photon AQGCs have only recently become available [15,19]. To illustrate the typical size of the limits that can be obtained for the AQGCs at a 500 GeV LC with 50 fb^{-1}, the following 1σ bounds have been extracted from the total cross section measurement of $e^+e^- \to u\overline{d}\mu^-\overline{\nu}_\mu + \gamma$, with all bounds in units of 10^{-3} GeV^{-2} [15]:

$$-0.12 < \frac{a_0}{\Lambda^2} < 0.14 \qquad -0.31 < \frac{a_c}{\Lambda^2} < 0.16 \qquad -0.82 < \frac{a_n}{\Lambda^2} < 0.79$$

$$-0.10 < \frac{\tilde{a}_0}{\Lambda^2} < 0.10 \qquad -0.69 < \frac{\tilde{a}_n}{\Lambda^2} < 0.90 \ . \qquad (5.2)$$

The availability of MC programs [15,19,23] will allow more detailed studies to be performed. For example, longitudinally polarized gauge bosons have the greatest effect on AQGCs, and gauge bosons with this polarization can be isolated through an analysis of gauge boson production and decay angles [21].

3 Strongly coupled theories

The Standard Model with a light Higgs boson provides a good fit to the electroweak data. Nevertheless, the electroweak observables depend only logarithmically on the Higgs mass, so that the effects of the light Higgs could be mimicked by new particles with masses as large as several TeV. A recent review of such scenarios is given in [26]. One can even imagine that no Higgs boson exists. In that case, the electroweak symmetry should be broken by some other interactions, and gauge boson scattering should become strong at a scale of order 1 TeV. An often discussed class of theories of this kind is called technicolor [27], which is discussed in the next subsection.

Electroweak symmetry is often assumed to be either connected to supersymmetry or driven by some strong dynamics, such as technicolor, without a Higgs boson. There is, however, a distinctive alternative where a strong interaction gives rise to bound states that include a Higgs boson. The latter could be light and weakly coupled at the electroweak scale. At sub-TeV energies these scenarios are described by a (possibly extended) Higgs sector, while the strong dynamics manifests itself only above a TeV or so.

3.1 Strong WW scattering and technicolor

The generic idea of technicolor theories is that a new gauge interaction, which is asymptotically free, becomes strong at a scale of order 1 TeV, such that the new fermions ("technifermions") that feel this interaction form condensates that break the electroweak symmetry. This idea is based on the observed dynamics of QCD, but arguments involving the fits to the electroweak data and the generation of quark masses suggest that the technicolor interactions should be described by a strongly coupled gauge theory that has a different behavior from QCD (see, *e.g.*, [28]).

A generic prediction of technicolor theories is that there is a vector resonance with mass below about 2 TeV which unitarizes the WW scattering cross section. In what follows we will concentrate on the capability of a linear e^+e^- collider of studying WW scattering, but first we briefly mention other potential signatures associated with various technicolor models. The chiral symmetry of the technifermions may be

large enough that its dynamical breaking leads to pseudo-Goldstone bosons, which are pseudoscalar bound states that can be light enough to be produced at a linear e^+e^- collider (for a recent study, see [29]). The large top-quark mass typically requires a special dynamics associated with the third generation. A thoroughly studied model along these lines is called Topcolor Assisted Technicolor [30], and leads to a rich phenomenology. This model predicts the existence of spinless bound states with large couplings to the top quark, called top-pions and top-Higgs, which may be studied at a linear e^+e^- collider [31].

Strong W^+W^- scattering is an essential test not only of technicolor theories, but in fact of any model that does not include a Higgs boson with large couplings to gauge boson pairs. It can be studied at a linear collider with the reactions $e^+e^- \to \nu\overline{\nu}W^+W^-$, $\nu\overline{\nu}ZZ$, $\nu\overline{\nu}t\overline{t}$, and W^+W^- [32]. The final states $\nu\overline{\nu}W^+W^-$, $\nu\overline{\nu}ZZ$ are used to study the I=J=0 channel in W^+W^- scattering, while the final state W^+W^- is best suited for studying the I=J=1 channel. The $\nu\overline{\nu}t\overline{t}$ final state can be used to investigate strong electroweak symmetry breaking in the fermion sector through the process $W^+W^- \to t\overline{t}$.

The first step in studying strong W^+W^- scattering is to separate the scattering of a pair of longitudinally polarized W's, denoted by $W_{\rm L}W_{\rm L}$, from transversely polarized W's, and from background such as $e^+e^- \to e^+e^-W^+W^-$ and $e^-\overline{\nu}W^+Z$. Studies have shown that simple cuts can be used to achieve this separation in $e^+e^- \to \nu\overline{\nu}W^+W^-$, $\nu\overline{\nu}ZZ$ at $\sqrt{s} = 1000$ GeV, and that the signals are comparable to those obtained at the LHC [33]. Furthermore, by analyzing the gauge boson production and decay angles it is possible to use these reactions to measure chiral Lagrangian parameters with an accuracy greater than that which can be achieved at the LHC [34].

The reaction $e^+e^- \to \nu\overline{\nu}t\overline{t}$ provides unique access to $W^+W^- \to t\overline{t}$, since this process is overwhelmed by the background $gg \to t\overline{t}$ at the LHC. Techniques similar to those employed to isolate $W_{\rm L}W_{\rm L} \to W^+W^-, ZZ$ can be used to measure the enhancement in $W_{\rm L}W_{\rm L} \to t\overline{t}$ production [35]. Even in the absence of a resonance it will be possible to establish a clear signal. The ratio $S/\sqrt{B}$ is expected to be 12 for a linear collider with $\sqrt{s} = 1$ TeV and 1000 fb^{-1} and 80%/0% electron/positron beam polarization, increasing to 28 for the same data sample at 1500 GeV.

There are two approaches to studying strong W^+W^- scattering with the process $e^+e^- \to W^+W^-$. The first approach was discussed in Section 2: a strongly coupled gauge boson sector induces anomalous TGCs that could be measured in $e^+e^- \to W^+W^-$. The precision of 4×10^{-4} for the TGCs κ_γ and κ_Z at $\sqrt{s} = 500$ GeV can be interpreted as a precision of 0.26 for the chiral Lagrangian parameters L_{9L} and L_{9R}. Assuming naive dimensional analysis [36], such a measurement would provide a 8σ (5σ) signal for L_{9L} and L_{9R} if the strong symmetry breaking energy scale were 3 TeV (4 TeV). The only drawback to this approach is that the detection of anomalous TGCs does not by itself provide unambiguous proof of strong electroweak symmetry breaking.

The second approach involves an effect unique to strong W^+W^- scattering. When W^+W^- scattering becomes strong the amplitude for $e^+e^- \to W_L W_L$ develops a complex form factor F_T in analogy with the pion form factor in $e^+e^- \to \pi^+\pi^-$ [37]. To evaluate the size of this effect the following expression for F_T has been suggested:

$$F_T = \exp\left[\frac{1}{\pi}\int_0^\infty ds'\delta(s', M_\rho, \Gamma_\rho)\left\{\frac{1}{s'-s-i\epsilon} - \frac{1}{s'}\right\}\right]$$

where

$$\delta(s, M_\rho, \Gamma_\rho) = \frac{1}{96\pi}\frac{s}{v^2} + \frac{3\pi}{8}\left[\tanh(\frac{s-M_\rho^2}{M_\rho\Gamma_\rho}) + 1\right] .$$

Here M_ρ, Γ_ρ are the mass and width, respectively, of a vector resonance in $W_L W_L$ scattering. The term

$$\delta(s) = \frac{1}{96\pi}\frac{s}{v^2}$$

is the Low Energy Theorem (LET) amplitude for $W_L W_L$ scattering at energies below a resonance. Below the resonance, the real part of F_T is proportional to $L_{9L} + L_{9R}$ and can therefore be interpreted as a TGC. The imaginary part, however, is a distinct new effect.

The real and imaginary parts of F_T are measured [38] in the same manner as the TGCs. The W^+W^- production and decay angles are analyzed, and an electron beam polarization of 80% is assumed. In contrast to TGCs, the analysis of F_T seems to benefit from even small amounts of jet flavor tagging. We therefore assume that charm jets can be tagged with a purity/efficiency of 100/33%. These purity/efficiency numbers are based on research [39] that indicates that it may be possible to tag charm jets with a purity/efficiency as high as 100/65%, given that b-jet contamination is not a significant factor in W^+W^- pair production and decay.

The expected 95% confidence level limits for F_T for $\sqrt{s} = 500$ GeV and a luminosity of 500 fb^{-1} are shown in Fig. 5.3, along with the predicted values of F_T for various masses M_ρ of a vector resonance in $W_L W_L$ scattering. The masses and widths of the vector resonances are chosen to coincide with those used in the ATLAS TDR [8]. The technipion form factor F_T affects only the amplitude for $e^+e^- \to W_L W_L$, whereas TGCs affect all amplitudes. Through the use of electron beam polarization and the rich angular information in W^+W^- production and decay, it will be possible to disentangle anomalous values of F_T from other anomalous TGC values and to deduce the mass of a strong vector resonance well below threshold, as suggested by Fig. 5.3.

The signal significances obtained by combining the results for $e^+e^- \to \nu\overline{\nu}W^+W^-$, $\nu\overline{\nu}ZZ$ [33] with the F_T analysis of W^+W^- [38] are displayed in Fig. 5.4 along with the results expected from the LHC [8]. The LHC signal is a mass bump in W^+W^-; the LC signal is less direct. Nevertheless, the signals at the LC are strong, particularly in $e^+e^- \to W^+W^-$, where the technirho effect gives a large enhancement of a very well-understood Standard Model process. Since the technipion form factor includes
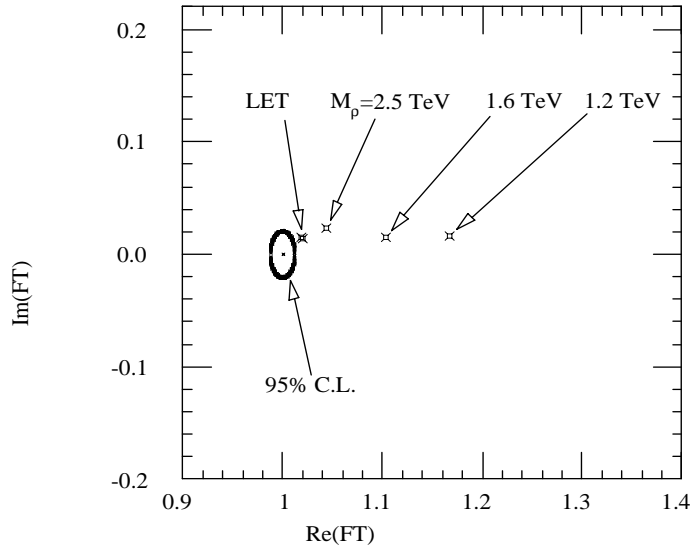
Figure 5.3: 95% C.L. contour for F_T for $\sqrt{s} = 500$ GeV and 500 fb^{-1}. Values of F_T for various masses M_ρ of a vector resonance in $W_\mathrm{L}W_\mathrm{L}$ scattering are also shown. The F_T point "LET" refers to the case where no vector resonance exists at any mass in strong $W_\mathrm{L}W_\mathrm{L}$ scattering.

an integral over the technirho resonance region, the linear collider signal significance is relatively insensitive to the technirho width. (The real part of F_T remains fixed as the width is varied, while the imaginary part grows as the width grows.) The LHC signal significance will drop as the technirho width increases. The large linear collider signals can be utilized to study a vector resonance in detail; for example, the evolution of F_T with $\hat{s}$ can be determined by measuring the initial-state radiation in $e^+e^- \to W^+W^-$.

Only when the vector resonance disappears altogether (the LET case in the lower right-hand panel in Fig. 5.4) does the direct strong symmetry breaking signal from the $\sqrt{s} = 500$ GeV linear collider drop below the LHC signal. At higher e^+e^- center-of-mass energies the linear collider signal exceeds the LHC signal.

3.2   Composite Higgs models

The good fit of the Standard Model to the electroweak data suggests that the new physics has a decoupling limit in which the new particles carrying $SU(2)_W \times U(1)_Y$ charges can be much heavier than the electroweak scale without affecting the Standard Model. This is the reason why the Minimal Supersymmetric Standard Model is viable: all the superpartners and the states associated with a second Higgs doublet can be taken to be heavier than the electroweak scale, leaving a low-energy theory given by
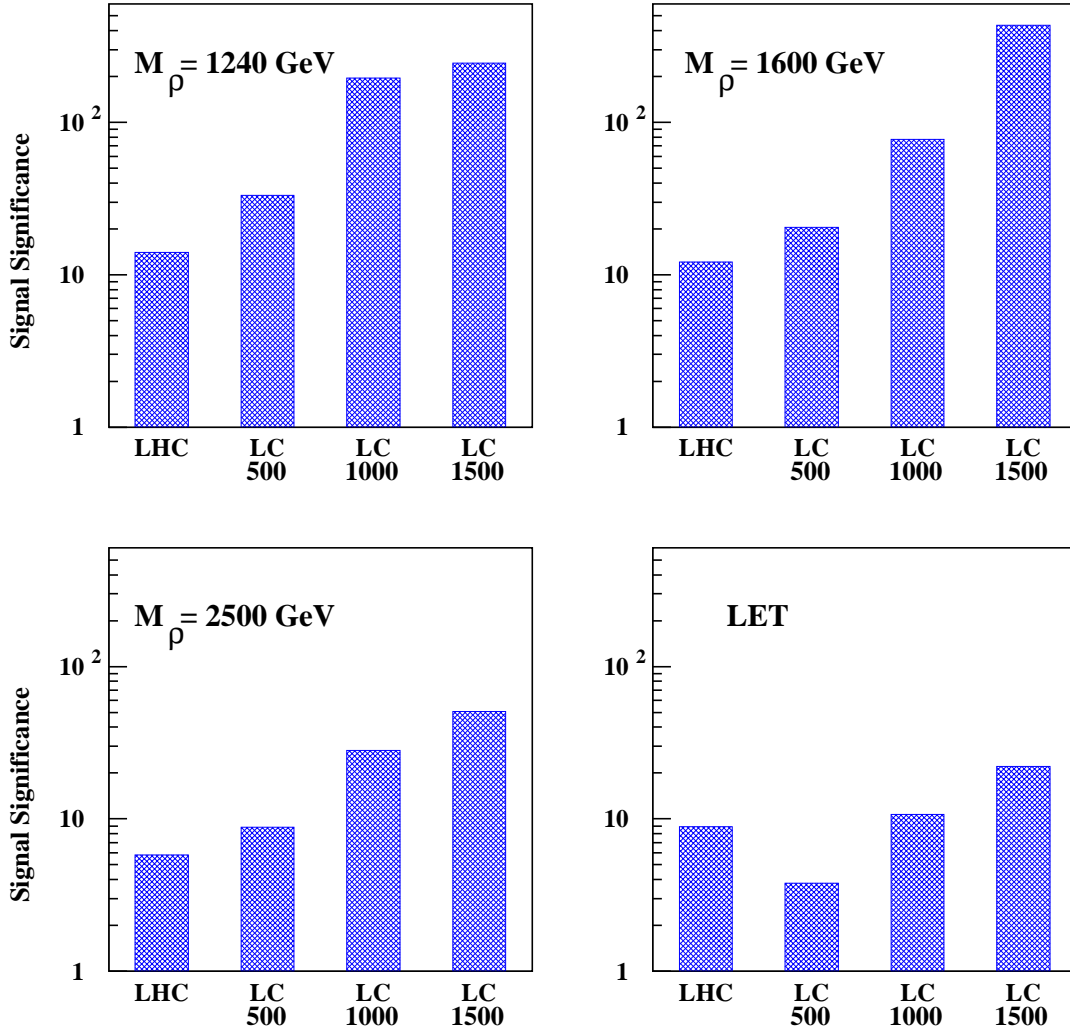
Figure 5.4: Direct strong symmetry breaking signal significance in σ's for various masses M_ρ of a vector resonance in $W_L W_L$ scattering. In the first three plots the signal at the LHC is a bump in the WW cross section; in the LET plot, the LHC signal is an enhancement over the SM cross section. The various LC signals are for enhancements of the amplitude for pair production of longitudinally polarized W bosons. The numbers below the "LC" labels refer to the center-of-mass energy of the linear collider in GeV. The luminosity of the LHC is assumed to be 300 fb^{-1}, while the luminosities of the linear colliders are assumed to be 500, 1000, and 1000 fb^{-1} for $\sqrt{s}$=500, 1000, and 1500 GeV respectively. The lower right hand plot "LET" refers to the case where no vector resonance exists at any mass in strong $W_L W_L$ scattering.

199

the Standard Model. At the same time, it is hard to construct viable technicolor models because they do not have a decoupling limit: the new fermions that condense and give the W and Z masses are chiral, *i.e.*, their masses break the electroweak symmetry.

There is a class of models of electroweak symmetry breaking that have a decoupling limit given by the Standard Model, so they are phenomenologically viable, and yet the Higgs field arises as a bound state due to some strong interactions. An example of such a composite Higgs model is the Top Quark Seesaw Theory, in which a Higgs field appears as a bound state of the top quark with a new heavy quark. This has proven phenomenologically viable and free of excessive fine-tuning [40]. Furthermore, the top quark is naturally the heaviest Standard Model fermion in this framework, because it participates directly in the breaking of the electroweak symmetry.

The interaction responsible for binding the Higgs field is provided by a spontaneously broken gauge symmetry, such as topcolor [41], or some flavor or family symmetry [42]. Such an interaction is asymptotically free, allowing for a solution to the hierarchy problem. At the same time the interaction is non-confining, and therefore has a very different behavior from the technicolor interaction discussed in the first part of this section.

Typically, in the top quark seesaw theory, the Higgs boson is heavy, with a mass of order 500 GeV [43]. However, the effective theory below the compositeness scale may include an extended Higgs sector, in which case the mixing between the CP-even scalars could bring the mass of the Standard Model-like Higgs boson down to the current LEP limit [40,44]. One interesting possibility in this context is that there is a light Higgs boson with nearly standard couplings to fermions and gauge bosons, but whose decay modes are completely non-standard. This happens whenever a CP-odd scalar has a mass less than half the Higgs mass and the coupling of the Higgs to a pair of CP-odd scalars is not suppressed. The Higgs boson decays in this case into a pair of CP-odd scalars, each of them subsequently decaying into a pair of Standard Model particles with model-dependent branching fractions [45]. If the Higgs boson has Standard Model branching fractions, then the capability of an e^+e^- linear collider depends on M_H, as discussed in [46]. On the other hand, if the Higgs boson has non-standard decays, an e^+e^- collider may prove very useful in disentangling the composite nature of the Higgs boson, by measuring its width and branching fractions.

The heavy-quark constituent of the Higgs has a mass of a few TeV, and the gauge bosons associated with the strong interactions that bind the Higgs are expected to be even heavier. Above the compositeness scale there must be some additional physics that leads to the spontaneous breaking of the gauge symmetry responsible for binding the Higgs. This may involve new gauge dynamics [47], or fundamental scalars and supersymmetry. For studying these interesting strongly interacting particles, the e^+e^- collider should operate at the highest energy achievable.

Other models of Higgs compositeness have been proposed recently [48], and more

are likely to be constructed in the future. Another framework in which a composite Higgs boson arises from a strong interaction is provided by extra spatial dimensions accessible to the Standard Model particles; this is discussed in Section 6.

4   Contact interactions and compositeness

There is a strong historical basis for the consideration of composite models that is currently mirrored in the proliferation of fundamental particles. If the fermions have substructure, then their constituents are bound by a confining force at the mass scale Λ, which characterizes the radius of the bound states. At energies above Λ, the composite nature of fermions would be revealed by the break-up of the bound states in hard scattering processes. At lower energies, deviations from the Standard Model may be observed via form factors or residual effective interactions induced by the binding force. These composite remnants are usually parameterized by the introduction of contact terms in the low-energy Lagrangian. More generally, four-fermion contact interactions represent a useful parametrization of many types of new physics originating at high energy scales, and specific cases will be discussed throughout this chapter.

The lowest-order four-fermion contact terms are of dimension 6. A general helicity-conserving, flavor-diagonal, Standard Model-invariant parameterization can be written as [49]

$$\mathcal{L} = \frac{g_{\text{eff}}^2 \eta}{\Lambda^2} \left(\overline{q}\gamma^\mu q + \mathcal{F}_\ell \overline{\ell}\gamma^\mu \ell \right)_{L/R} \left(\overline{q}\gamma_\mu q + \mathcal{F}_\ell \overline{\ell}\gamma_\mu \ell \right)_{L/R} , \qquad (5.3)$$

where the generation and color indices have been suppressed, $\eta = \pm 1$, and $\mathcal{F}_\ell$ is inserted to allow for different quark and lepton couplings but is anticipated to be $\mathcal{O}(1)$. Since the binding force is expected to be strong when Q^2 approaches Λ^2, it is conventional to define $g_{\text{eff}}^2 = 4\pi$.

Interference between the contact terms and the usual gauge interactions can lead to observable deviations from Standard Model predictions at energies lower than Λ. Currents limits from various processes at the Tevatron and LEP II place Λ above the few-TeV range. At the LHC [8], $\Lambda_{\ell q}$ terms can be probed to $\sim 20 - 30$ TeV for integrated luminosities of $10-100$ fb^{-1}, while the Λ_{qq} case is more problematic because of uncertainties in the parton distributions and the extrapolation of the calorimeter energy calibration to very high values of the jet p_T.

At a LC, the use of polarized beams, combined with angular distributions, allows for a clear determination of the helicity of the contact term. An examination of contact effects in $e^+e^- \to f\overline{f}$, where $f = \mu, c, b$ was performed for LC energies in [50]. This study concentrated on tagged final states, since contact effects are diluted when all quark flavors are summed because of cancellations between the up- and down-type quarks. Here, both polarized and unpolarized angular distributions were

	Λ_{LL}	Λ_{LR}	Λ_{RL}	Λ_{RR}
$\sqrt{s} = 0.5$ TeV				
$e_L^- e^+ \rightarrow \mu^+ \mu^-$	57	52	18	18
$e_R^- e^+ \rightarrow \mu^+ \mu^-$	20	18	52	55
$e_L^- e^+ \rightarrow c\bar{c}$	59	50	9	15
$e_R^- e^+ \rightarrow c\bar{c}$	21	20	43	57
$e_L^- e^+ \rightarrow b\bar{b}$	68	53	9	16
$e_R^- e^+ \rightarrow b\bar{b}$	30	21	59	59
$\sqrt{s} = 1.0$ TeV				
$e_L^- e^+ \rightarrow \mu^+ \mu^-$	79	72	25	26
$e_R^- e^+ \rightarrow \mu^+ \mu^-$	28	25	73	78
$e_L^- e^+ \rightarrow c\bar{c}$	82	72	12	21
$e_R^- e^+ \rightarrow c\bar{c}$	30	28	62	78
$e_L^- e^+ \rightarrow b\bar{b}$	94	77	14	23
$e_R^- e^+ \rightarrow b\bar{b}$	43	30	82	84

Table 5.3: 95% CL search reach in TeV for contact interaction scales with various helicities.

examined with tagging efficiencies of 60% and 35% for b- and c-quarks, respectively, and the detector acceptance was taken to be $|\cos\theta| < 0.985$. The resulting 95% CL sensitivity for $\mathcal{L} = 500$ fb^{-1} to Λ from the polarized distributions with 90% electron beam polarization is listed in Table 5.3.

Compositeness limits for Λ_{LL}^+ from Møller and Bhabha scattering [51] are summarized in Fig. 5.5. For equal luminosities the limits from Møller scattering are significantly better than those from Bhabha scattering. This is due not only to the polarization of both beams, but also to the Møller/Bhabha crossing relation in the central region of the detector. Limits on Λ_{LL}^+ for different energies and luminosities can be calculated under the assumption that the compositeness limit scales as $\mathcal{L}^{1/4} s^{1/2}$.

5 New particles in extended gauge sectors and GUTs

5.1 Extended gauge sectors

New gauge bosons are a feature of many extensions of the Standard Model. They arise naturally in grand unified theories, such as $SO(10)$ and E_6, where the GUT group gives rise to extra $U(1)$ or $SU(2)$ subgroups after decomposition. There are also numerous non-unified extensions, such as the Left-Right Symmetric model and Topcolor. More recently, there has been renewed interest in Kaluza-Klein excitations of the SM gauge bosons, which are realized in theories of extra space dimensions at semi-macroscopic scales. All of these extensions of the SM predict the existence of
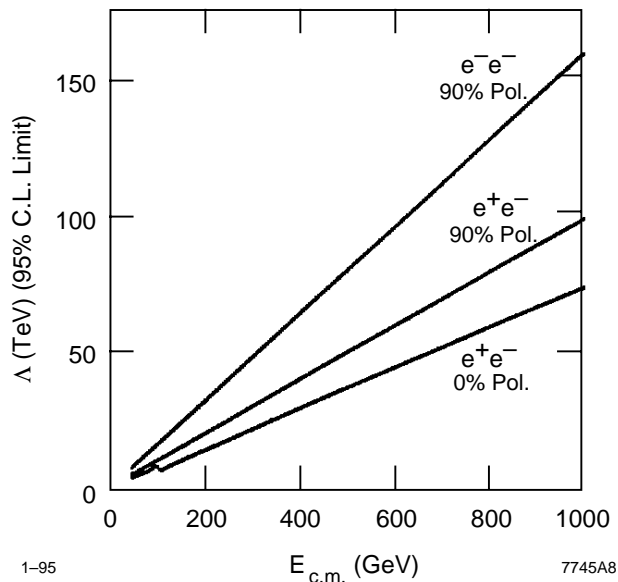
Figure 5.5: The 95% confidence level limits for the compositeness scale Λ_{LL}^+ from Møller and Bhabha scattering as a function of the e^-e^- or e^+e^- center-of-mass energy. The luminosity is given by $\mathcal{L} = 680 \text{ pb}^{-1} \cdot s/M_Z^2$. The polarization of the electron beam(s) is indicated in the figure.

new gauge bosons, generically denoted as Z' or W'. The search for extra gauge bosons thus provides a common coin in the quest for new physics at high-energy colliders. Here, we concentrate on the most recent developments on the subject, and refer the interested to recent reviews [52].

5.1.1 Z' discovery limits and identification

The signal for the existence of a new neutral gauge boson at linear collider energies arises through the indirect effects of s-channel Z' exchange. Through its interference with the SM γ and Z exchange in $e^+e^- \to f\overline{f}$, significant deviations from SM predictions can occur even when $M_{Z'}$ is much larger than $\sqrt{s}$. This sensitivity to the Z' nicely complements the ability of the LHC to discover a Z' as a resonance in lepton pair production. The combination of many LC observables such as the cross sections for $f\overline{f}$ final states, forward-backward asymmetries, A_{FB}^f, and left-right asymmetries, A_{LR}^f, where $f = \mu,\ \tau,\ c,\ b$, and light quarks, can fill in the detailed picture of the Z' couplings.

The combined sensitivity of the LC measurements for various Z' models is shown in Fig. 5.6 [52]. We see that if a Z' is detected at the LHC, precision measurements at the LC could be used to measure its properties and determine the underlying theory.

NLC (e⁺ e⁻)

$\sqrt{s}$=0.5 TeV, L=50fb⁻¹

$\sqrt{s}$=1 TeV L=200fb⁻¹

$\sqrt{s}$=1.5 TeV, L=200fb⁻¹

LHC (pp)
$\sqrt{s}$=14 TeV, L=10fb⁻¹

$\sqrt{s}$=14 TeV, L=100fb⁻¹

Z_χ
Z_ψ
Z_η
Z_{LR}
Z_{ALR}
Z_{SSM}
Z_{HARV}

1000   10000

Discovery Reach for Z'   (GeV)
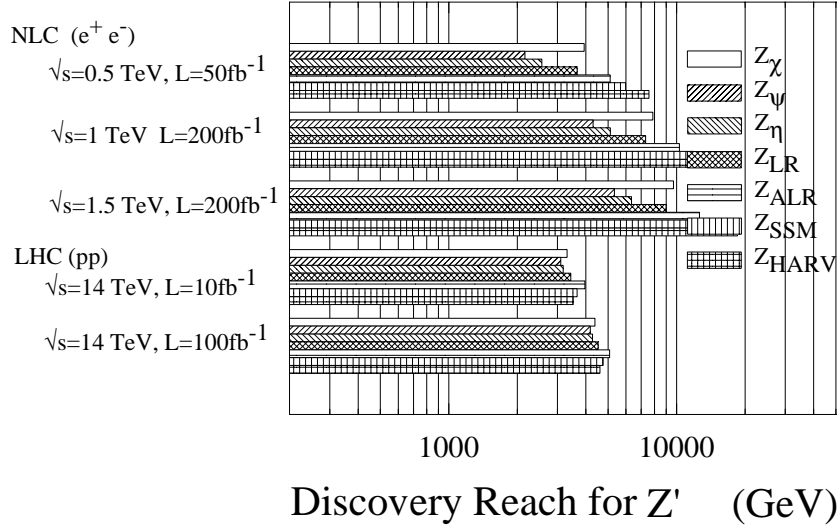
Figure 5.6: 95% CL search limits for extra neutral gauge bosons, for various models, at high-energy linear colliders, by observation of corrections to $e^+e^- \to f\overline{f}$ processes, and at the LHC, by observation of a peak in dilepton pairs.

Figure 5.7 displays the resolving power between Z' models assuming that the mass of the Z' was measured previously at the LHC. This study only considers leptonic final states and assumes lepton universality. If $M_{Z'}$ were beyond the LHC discovery reach or if the Z' does not couple to quarks then no prior knowledge of it would be obtained before the LC turns on. However, in this case, the LC can still yield some information on the Z' couplings and mass. Instead of extracting Z' couplings directly, "normalized" couplings, defined by

$$a_f^N = a'_f \sqrt{\frac{s}{M_{Z'}^2 - s}}; \quad v_f^N = v'_f \sqrt{\frac{s}{M_{Z'}^2 - s}} \tag{5.4}$$

could be measured. For a demonstration of this case, the diagnostic power of a 1 TeV LC for a Z' with couplings of the E_6 model χ and mass $M_{Z'} = 5$ TeV is displayed in Fig. 5.7 for $f = \ell$. An additional determination of the Z' mass and couplings could be performed [52] in this case from cross section and asymmetry measurements at several different values of $\sqrt{s}$.

A recent study of the process $e^+e^- \to \nu\overline{\nu}\gamma$ has demonstrated that the process can also be used to obtain information on $Z' - \nu\overline{\nu}$ couplings [53].

5.1.2 W' discovery limits and identification

While considerable effort has been devoted to the study of Z' bosons at e^+e^- colliders, a corresponding endeavor for the W' sector has only recently been undertaken. A
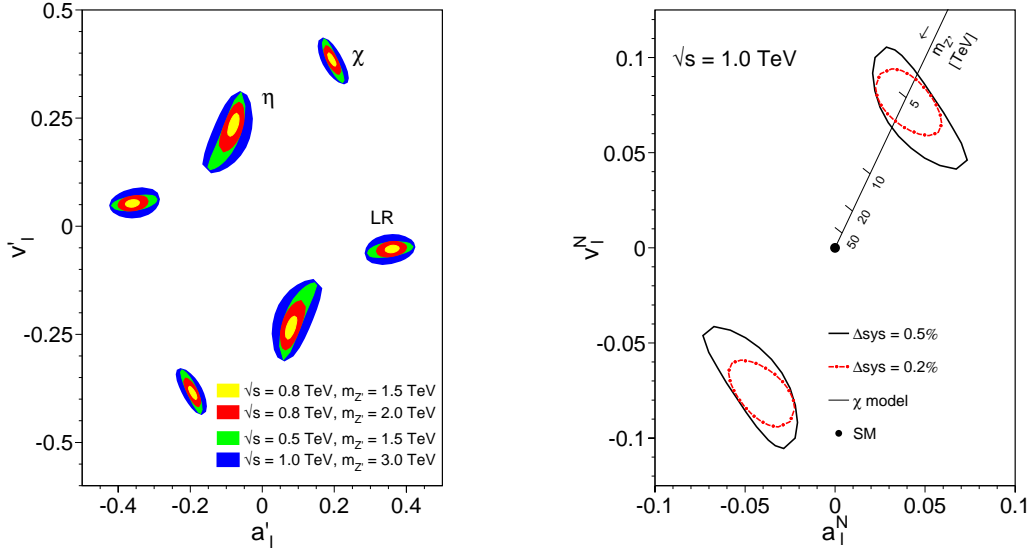
Figure 5.7: Left Panel: Resolution power (95% C.L.) for different $M_{Z'_\chi}$ based on measurements of leptonic observables at $\sqrt{s} = 1$ TeV with a luminosity of $L_{\text{int}} = 1$ ab^{-1} [56]. Right Panel: Resolution power (95% C.L.) for different $M_{Z'}$ based on measurements of leptonic observables at $\sqrt{s} = 500$ GeV, 800 GeV, 1 TeV with a luminosity of $L_{\text{int}} = 1$ ab^{-1}. The leptonic couplings of the Z' correspond to the χ, η, or LR model [56].

preliminary investigation [54] of the sensitivity of $e^+e^- \to \nu\bar{\nu}\gamma$ to W' bosons was performed at Snowmass 1996, and more detailed examinations [53,55] have recently been performed. The models with extra $SU(2)$ factors considered in these studies are the Left-Right symmetric model (LRM) based on the gauge group $SU(2)_L \times SU(2)_R \times U(1)_{B-L}$, the Un-Unified model (UUM) based on $SU(2)_q \times SU(2)_l \times U(1)_Y$ where the quarks and leptons each transform under their own $SU(2)$, a Third Family Model (3FM) based on the group $SU(2)_h \times SU(2)_l \times U(1)_Y$ where the quarks and leptons of the third (heavy) family transform under a separate group, and the KK model which contains the Kaluza-Klein excitations of the SM gauge bosons that are a possible consequence of theories with large extra dimensions.

In the process $e^+e^- \to \nu\bar{\nu}\gamma$, both charged and neutral extra gauge bosons can contribute. In the analysis of [53], the photon energy and angle with respect to the beam axis are restricted to $E_\gamma \geq 10$ GeV and $10° \leq \theta_\gamma \leq 170°$, to take into account detector acceptance. The most serious background, radiative Bhabha scattering in which the scattered e^+ and e^- go undetected down the beam pipe, is suppressed by restricting the photon's transverse momentum to $p_T^\gamma > \sqrt{s} \sin\theta_\gamma \sin\theta_v/(\sin\theta_\gamma + \sin\theta_v)$, where θ_v is the minimum angle at which the veto detectors may observe electrons or positrons; here, $\theta_v = 25$ mrad. The observable $d\sigma/dE_\gamma$ was found to provide the most statistically significant search reach. The 95% CL reach is displayed graphically in Fig. 5.8 and in Table 5.4, which shows the degradation when a 2% systematic error

is added in quadrature with the statistical error. The corresponding W' search reach at the LHC is in the range 5–6 TeV [52].
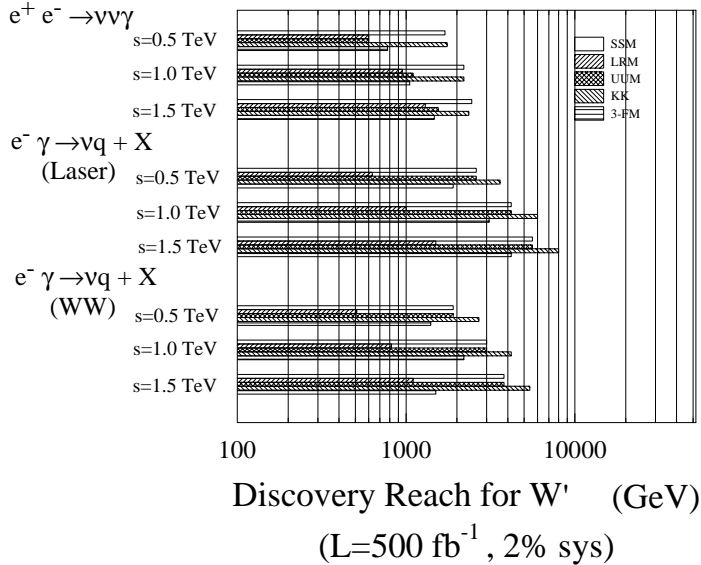
Figure 5.8: 95% CL search limits for W' bosons at the LC.

The 95% CL constraints that can be placed on the right- and left-handed couplings of a W' to fermions, assuming that the W' has Standard Model-like couplings, and that there is no corresponding Z' contribution to $e^+e^- \to \nu\bar{\nu}\gamma$, are shown in Fig. 5.9. Here, the total cross section σ and the left-right asymmetry A_{LR} are used as observables, with the systematic errors for $\sigma(A_{LR})$ taken as 2%(1%) and 80% electron and 60% positron polarization are assumed. The axes in this figure correspond to couplings normalized as $L_f(W) = C_L^{W'} g/(2\sqrt{2})$ and similarly for $R_f(W)$. It is found that 2% systematic errors dominate the coupling determination. In addition, we note that the W' couplings can only be constrained up to a two-fold ambiguity, which could be resolved by reactions in which the W' couples to a triple gauge vertex.

Additional sensitivity to the existence of a W' can be gained from $e\gamma \to \nu q + X$ [55]. This process receives contributions only from charged and not from neutral gauge bosons. The W' contribution can be isolated by imposing a kinematic cut requiring either the q or $\overline{q}$ to be collinear to the beam axis. In order to take into account detector acceptance, the angle θ_q of the detected quark relative to the beam axis is restricted to $10° \leq \theta_q \leq 170°$. The kinematic variable that is most sensitive to a W' is the p_{T_q} distribution. The quark's transverse momentum relative to the beam is restricted to $p_T^q > 40(75)$ GeV for $\sqrt{s} = 0.5(1.0)$ TeV, to suppress various Standard Model backgrounds. Figure 5.9 and Table 5.4 show the resulting 95% CL constraints on the W' fermionic couplings for the case of backscattered laser photons. As seen above, the assumed systematic error of 2% again dominates the statistical
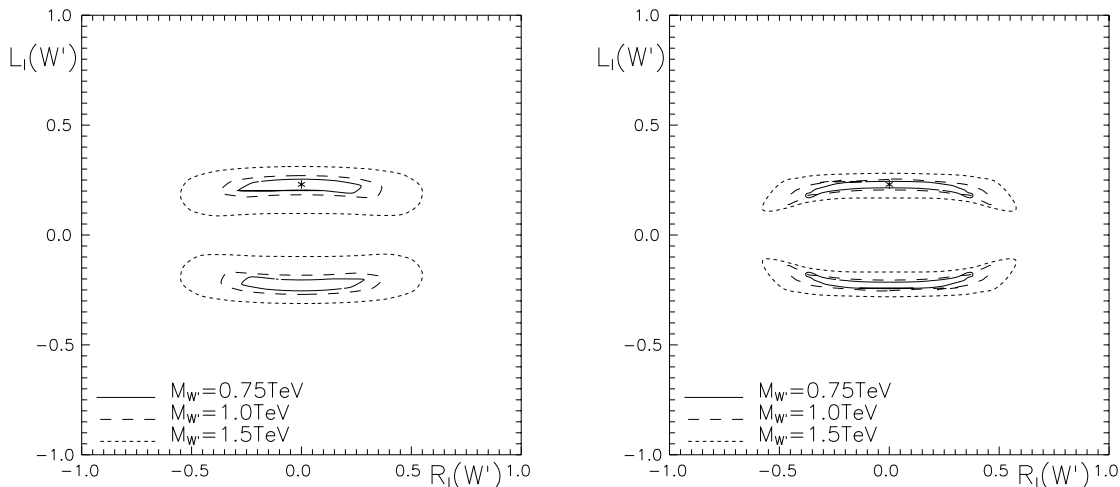
Figure 5.9: Left Panel: 95% CL constraints from $e^+e^- \to \nu\overline{\nu}\gamma$ on couplings of the SSM W' indicated by a star for $\sqrt{s} = 0.5$ TeV and $L_{\text{int}} = 1000$ fb^{-1} with a systematic error of 0.5% (0.25%) for $\sigma(A_{LR})$ for different W' masses. Right Panel: 95% C.L. constraints from $e\gamma \to \overline{\nu}q + X$ on couplings of the SSM W' for $\sqrt{s} = 0.5$ TeV and $L_{\text{int}} = 1000$ fb^{-1} with a 2% systematic error for different W' masses.

| | $\sqrt{s} = 0.5$ TeV, $L_{\text{int}} = 500$ fb^{-1} | | | | $\sqrt{s} = 1$ TeV, $L_{\text{int}} = 500$ fb^{-1} | | | |
| | $e^+e^- \to \nu\overline{\nu}\gamma$ | | $e\gamma \to \nu q + X$ | | $e^+e^- \to \nu\overline{\nu}\gamma$ | | $e\gamma \to \nu q + X$ | |
Model	no syst.	syst.	no syst	syst.	no syst.	syst.	no syst.	syst.
SSM W'	4.3	1.7	4.1	2.6	5.3	2.2	5.8	4.2
LRM	1.2	0.6	0.8	0.6	1.6	1.1	1.2	1.1
UUM	2.1	0.6	4.1	2.6	2.5	1.1	5.8	4.2
KK	4.6	1.8	5.7	3.6	5.8	2.2	8.3	6.0
3FM	2.3	0.8	3.1	1.9	2.7	1.1	4.4	3.1

Table 5.4: 95% CL search limits for W' bosons, in TeV, for various reactions.

error, thus eliminating the potential gain from high luminosities. W' coupling determination from backscattered laser photons are considerably better than those from Weizsäcker-Williams photons or from e^+e^- collisions. Polarized beams give only a minor improvement to these results after the inclusion of systematic errors.

If a W' were discovered elsewhere, measurements of its couplings in both $e^+e^- \to \nu\overline{\nu}\gamma$ and $e\gamma \to \nu q + X$ could provide valuable information regarding the underlying model, with the latter process serving to isolate the W' couplings from those of the Z'.

5.2 Leptoquarks

Leptoquarks are natural in theories that relate leptons and quarks at a more fundamental level. These spin-0 or -1 particles carry both baryon and lepton number and are color triplets under $SU(3)_C$. They can be present at the electroweak scale in models where baryon and lepton number are separately conserved, thus avoiding conflicts with rapid proton decay. Their remaining properties depend on the model in which they appear, and would need to be determined in order to ascertain the framework of the underlying theory. Given the structure of the Standard Model fermions, there are 14 different possible types of leptoquarks; their classification can be found in [57]. Their fermionic couplings proceed through a Yukawa interaction of unknown strength, while their gauge couplings are specified for a particular leptoquark. Low-energy data place tight constraints on intergenerational leptoquark Yukawa couplings and also require that these couplings be chiral. A summary of the current state of experimental searches for leptoquarks is given in [58].

At a linear collider, leptoquarks may be produced in pairs or as single particles, while virtual leptoquark exchange may be present in $e^+e^- \rightarrow$ hadrons. Pair production receives a t-channel quark-exchange contribution whose magnitude depends on the size of the Yukawa coupling. This only competes with the usual s-channel exchange, which depends on the leptoquark's gauge couplings, if the Yukawa coupling is of order electromagnetic strength. The possible signatures are e^+e^-, $e^{\pm}$ plus missing E_T, or missing E_T alone, combined with two jets. The observation is straightforward essentially up to the kinematic limit. A thorough study of the background and resulting search reach for each type of leptoquark can be found in [59]. Single leptoquark production is most easily studied in terms of the quark content of the photon [60]. In this case a lepton fuses with a quark from a Weiszäcker-Williams photon (in e^+e^- mode) or a laser-backscattered photon (in $e\gamma$ mode) to produce a leptoquark. The cross section is a convolution of the parton-level process with distribution functions for the photon in the electron and the quark in the photon, and is directly proportional to the $eqLQ$ Yukawa coupling. The kinematic advantage of single production is lost if the Yukawa coupling is too small. For Yukawa couplings of electromagnetic strength, leptoquarks with mass up to about 90% of $\sqrt{s}$ can be discovered at a LC [60]. If the Yukawa couplings are sizable enough, then virtual leptoquark exchange [61] will lead to observable deviations in the hadronic production cross section for leptoquark masses in excess of $\sqrt{s}$. A summary of the search reach from these three processes is shown in Fig. 5.10 from [59] in the leptoquark mass-coupling plane. In comparison, leptoquarks are produced strongly at the LHC, with search reaches in the 1.5 TeV range [62] independent of the Yukawa couplings.

The strength of the LC is in the determination of the leptoquark's electroweak quantum numbers and the strength of its Yukawa couplings once it is discovered. Together, the production rate and polarized left-right asymmetry can completely de-
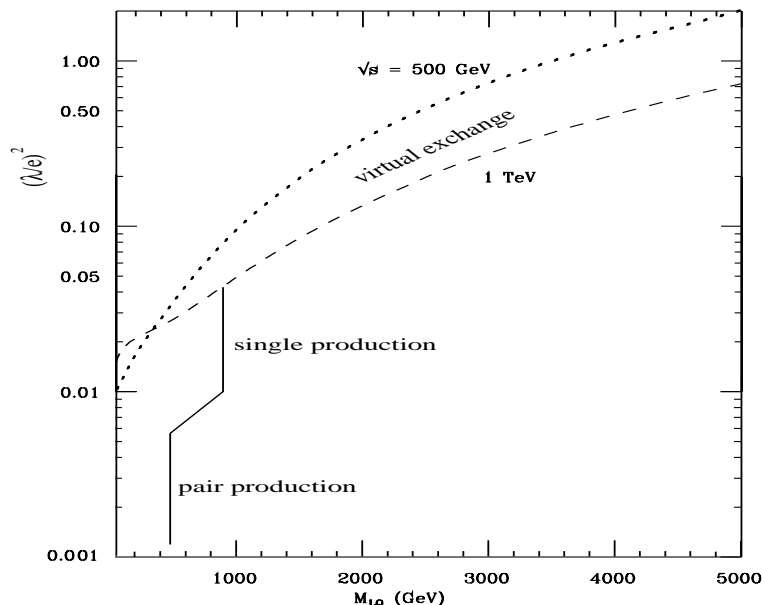
Figure 5.10: Leptoquark search limits at a LC from the three processes discussed in the text. The Yukawa coupling is scaled to e. The pair- and single-production reaches are shown for $\sqrt{s} = 1$ TeV, while the indirect reach is displayed for $\sqrt{s} = 0.5$ and 1 TeV.

termine the leptoquark's electroweak properties and identify its type [63] in both the pair and single production channels, up to the kinematic limit. In addition, the Yukawa coupling strength can be measured via the forward-backward asymmetry in leptoquark pair production (which is non-vanishing for significant Yukawa couplings), deviations in the hadronic cross sections, and the comparison of pair and single production rates.

5.3 Exotic fermions

Fermions beyond the ordinary Standard Model content arise in many extensions of the Standard Model, notably in grand unified theories. They are referred to as exotic fermions if they do not have the usual $SU(2)_L \times U(1)_Y$ quantum numbers. For a review, we refer the reader to [64]. Examples of new fermions are the following: (*i*) The sequential repetition of a Standard Model generation (of course, in this case the fermions maintain their usual $SU(2)_L \times U(1)_Y$ assignments). (*ii*) Mirror fermions, which have chiral properties opposite to those of their Standard Model counterparts [65]. The restoration of left-right symmetry is a motivating factor for this possibility. (*iii*) Vector-like fermions that arise when a particular weak isospin representation is present for both left and right handed components. For instance, in E_6 grand unified theories, with each fermion generation in the representation of dimension 27, there are two additional isodoublets of leptons, one sequential (left-handed) and one mirror

209

(right-handed). This sort of additional content is referred to as a vector doublet model (VDM) [66], whereas the addition of weak isosinglets in both chiralities is referred to as a vector singlet model (VSM) [67].

Exotic fermions can mix with the Standard Model fermions; in principle, the mixing pattern may be complicated and is model-independent. One simplifying factor is that intergenerational mixing is severely limited by the constraints on flavor-changing neutral currents, as such mixing is induced at the tree level [66]. Thus most analyses neglect intergenerational mixing. Global fits of low-energy electroweak data and the high-precision measurements of the Z properties provide upper limits for the remaining mixing angles of the order of $\sin^2\theta_{\mathrm{mix}} \leq 10^{-2} - 10^{-3}$ [68].

Exotic fermions may be produced in e^+e^- collisions either in pairs or singly in association with their Standard Model partners as a result of mixing. The cross section for pair production of exotic quarks via gluon fusion and the Drell-Yan process at the LHC is large enough that the reach of the LC is unlikely to be competitive [69]. On the other hand, the backgrounds to exotic lepton production are large in pp collisions, with production in e^+e^- collisions providing a promising alternative. Generally, the search reach for exotic leptons is up to the kinematic limit of the e^+e^- machine, for allowed mixings [70]. The experimental signature requires knowledge of the $L^\pm$ decay mode, which is model-dependent and also depends on the mass difference of the charged and neutral exotic leptons. Studies indicate that the signals for exotic lepton production are clear and easy to separate from Standard Model backgrounds [64,70,71], and that the use of polarized beams is important in determining the electroweak quantum numbers [71].

Almeida *et al.* have recently presented a detailed study of neutral heavy lepton production at high-energy e^+e^- colliders [72]. They find single heavy neutrino production to be more important than pair production and have calculated the process $e^+e^- \to \nu e^\pm W^\mp$ including on-shell and off-shell heavy neutrinos. They conclude that e^+e^- colliders can test the existence of heavy Dirac and Majorana neutrinos up to $\sqrt{s}$ in the $\nu e^\pm +$ hadrons channel. Single heavy neutrino production can be clearly separated from Standard Model backgrounds, particularly with the application of angular cuts on the final-state particle distributions. Figure 5.11 shows the on-shell approximation cross sections for various pair- and single-production processes, with all mixing angles such that $\sin^2\theta_{\mathrm{mix}} = 0.0052$ [68].

6   Extra dimensions

The possibility has recently been proposed of utilizing the geometry of extra spatial dimensions to address the hierarchy problem, *i.e.*, the disparity between the electroweak and Planck scales [73,74]. This idea exploits the fact that gravity has yet to be probed at energy scales much above 10^{-3} eV in laboratory experiments, imply-
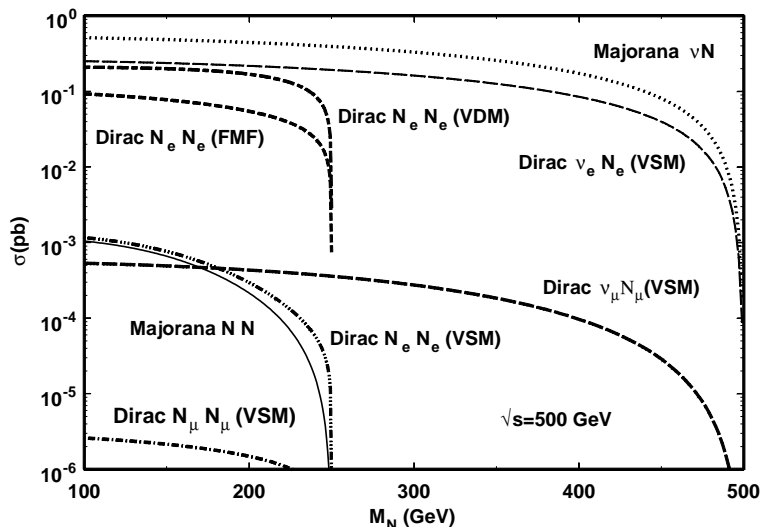
Figure 5.11: Single and pair production cross sections of on-shell heavy Dirac and Majorana neutrinos at $\sqrt{s} = 500$ GeV for e^+e^- colliders [72].

ing that the Planck scale (of order 10^{19} GeV), where gravity becomes strong, may not be fundamental but simply an artifact of the properties of the higher-dimensional space. In one such scenario [73], the apparent hierarchy is generated by a large volume for the extra dimensions, while in a second case [74], the observed hierarchy is created by an exponential function of the compactification radius of the extra dimension. An exciting feature of these theories is that they afford concrete and distinctive experimental tests both in high energy physics and in astrophysics. Furthermore, if they truly describe the source of the observed hierarchy, then their signatures should appear in high-energy experiments at the TeV scale.

Another possibility is the existence of TeV^{-1}-sized extra dimensions accessible to Standard Model fields. Although these theories do not explicitly address the hierarchy between the Electroweak and Planck scales, they are not ruled out experimentally and may arise naturally from string theory [75]. Furthermore, they serve as a mechanism for suppressing proton decay and generating the hierarchical pattern of fermion masses [76]. Models with TeV-scale extra dimensions provide a context for new approaches to the problem of explaining electroweak symmetry breaking [77,78] and the existence of three generations of quarks and leptons [79]. These theories also give rise to interesting phenomenology at the TeV scale.

We first describe some common features of these theories. In all the above scenarios, our universe lies on a 3+1-dimensional brane (sometimes called a wall) that is embedded in the higher $4 + \delta$-dimensional space, known as the bulk. The field content that is allowed to propagate in the bulk varies between the different models. Upon compactification of the additional dimensions, all bulk fields expand into a Kaluza-Klein (KK) tower of states on the $3 + 1$-dimensional brane, where the masses of the KK states are related to the δ-dimensional kinetic motion of the bulk field. It is the direct observation or indirect effects of the KK states that signal the existence of extra dimensions at colliders.

6.1 Large extra dimensions

In this scenario [73], gravitational fields propagate in the δ new large spatial dimensions, as well as in the usual $3 + 1$ dimensions. It is postulated that their interactions become strong at the TeV scale. The volume of the compactified dimensions, V_δ, relates the scale where gravity becomes strong in the $4 + \delta$-dimensional spaces to the apparent Planck scale via Gauss' Law

$$M_{Pl}^2 = V_\delta M_*^{2+\delta} \,, \tag{5.5}$$

where M_* denotes the fundamental Planck scale in the higher-dimensional space. Setting M_* to be of order $1 \sim$ TeV thus determines the compactification radius r_c $(V_\delta \sim r_c^\delta)$ of the extra dimensions, which ranges from a sub-millimeter to a few fermi for $\delta = 2$–6, assuming that all radii are of equal size. The compactification scale $(M_c = 1/r_c)$ associated with these parameters then ranges from 10^{-4} eV to a few MeV. The case of $\delta = 1$ (which yields $r_c \approx 10^{11}$ m) is immediately excluded by astronomical data. Cavendish-type experiments, which search for departures from the inverse-square law gravitational force, exclude [80] $r_c > 190$ μm for $\delta = 2$, which translates to the bound $M_* > 1.6$ TeV using the convention in [81]. In addition, astrophysical and cosmological considerations [82], such as the rate of supernova cooling and the diffuse γ ray spectrum, disfavor a value of M_* near the TeV scale for $\delta = 2$. Precision electroweak data [83] do not allow the Standard Model fields to propagate in extra dimensions with $M_c <$ a few TeV, and hence they are constrained to the $3 + 1$-dimensional brane in this model.

The Feynman rules for this scenario [81,84] are obtained by considering a linearized theory of gravity in the bulk. The bulk field strength tensor can be decomposed into spin-0, 1, and 2 states, each of which expands into KK towers upon compactification. These KK states are equally spaced and have masses of n/r_c where n labels the KK excitation level. Taking $M_* = 1$ TeV, we see that the KK state mass splittings are equal to 5×10^{-4} eV, 20 keV, and 7 MeV for $\delta = 2, 4$, and 6, respectively. The interactions of the KK gravitons with the Standard Model fields on the wall are governed by the conserved stress-energy tensor of the wall fields. The spin-1 KK

states do not interact with the wall fields because of the form of the wall stress-energy tensor. The non-decoupling scalar KK states couple to the trace of the stress-energy tensor, and are phenomenologically irrelevant for most collider processes. Each state in the spin-2 KK tower, G_n, couples identically to the Standard Model wall fields via their stress-energy tensor with the strength proportional to the inverse 4-dimensional Planck scale, M_{Pl}^{-1}. It is important to note that this description is an effective 4-dimensional theory, valid only for energies below M_*. The full theory above M_* is unknown.

Two classes of collider signatures arise in this model. The first is emission of the graviton KK tower states in scattering processes [81,85]. The relevant process at a linear collider is $e^+e^- \rightarrow \gamma/Z + G_n$, where the graviton appears as missing energy in the detector, behaving as if it were a massive, non-interacting, stable particle. The cross section is computed for the production of a single massive graviton excitation and then summed over the full tower of KK states. Since the mass splittings of the KK excitations are quite small compared to the collider center-of-mass energy, this sum can be replaced by an integral weighted by the density of KK states which is cut off by the specific process kinematics. The cross section for this process scales as simple powers of $\sqrt{s}/M_*$. It is important to note that because of the integral over the effective density of states, the emitted graviton appears to have a continuous mass distribution. This corresponds to the probability of emitting gravitons with different extra-dimensional momenta. The observables for graviton production, such as the γ/Z angular and energy distributions, are thus distinct from those of other new physics processes, such as supersymmetric particle production, since the latter corresponds to a fixed invisible particle mass. The Standard Model background transition $e^+e^- \rightarrow \nu\overline{\nu}\gamma$ also has different characteristics, since it is a three-body process.

The cross section for $e^+e^- \rightarrow \gamma G_n$ as a function of the fundamental Planck scale is presented in Fig. 5.12 for $\sqrt{s} = 1$ TeV. The level of Standard Model background is also shown, with and without electron beam polarization set at 90%. We note that the signal (background) increases (decreases) with increasing $\sqrt{s}$. Details of the various distributions associated with this process can be found in Cheung and Keung [85]. The discovery reach from this process has been computed in [86], with $\sqrt{s} = 800$ GeV, 1000 fb^{-1} of integrated luminosity, including various beam polarizations and kinematic acceptance cuts, ISR, and beamstrahlung. The results are displayed in Table 5.5. In this table, we have also included the 95% CL bounds obtained [87] at LEP for $\sqrt{s} > 200$ GeV.

The associated emission process at hadron colliders, $q\overline{q} \rightarrow g + G_n$, results in a mono-jet signal. In this case, the effective low-energy theory breaks down for some regions of the parameter space, as the parton-level center-of-mass energy can exceed the value of M_*. The experiment is then sensitive to the new physics appearing above M_*. An ATLAS simulation [88] of the missing transverse energy in signal and background events at the LHC with 100 fb^{-1} results in the discovery range for the

$e^+e^- \rightarrow \gamma + G_n$		2	4	6
LC	$P_{-,+} = 0$	5.9	3.5	2.5
LC	$P_- = 0.8$	8.3	4.4	2.9
LC	$P_- = 0.8,\ P_+ = 0.6$	10.4	5.1	3.3
LEP II		1.45	0.87	0.61
$pp \rightarrow g + G_n$		2	3	4
LHC		$4.0 - 8.9$	$4.5 - 6.8$	$5.0 - 5.8$

Table 5.5: 95% CL sensitivity to the fundamental Planck scale M_* in TeV for different values of δ, from the emission process for various polarization configurations and different colliders as discussed in the text. $\sqrt{s} = 800$ GeV and 1 ab^{-1} has been assumed for the LC and 100 fb^{-1} for the LHC.

effective theory displayed in Table 5.5. The lower end of the range corresponds to values at which the ultraviolet physics sets in and the effective theory fails, while the upper end represents the boundary where the signal is no longer observable above background.

If an emission signal is observed, one would like to determine the values of the fundamental parameters, M_* and δ. In this case, measurement of the cross section at a linear collider at two different values of $\sqrt{s}$ can be used to determine δ [86] and test the consistency of the data with the hypothesis of large extra dimensions. This is displayed for a LC in Fig. 5.13.

The second class of collider signals for large extra dimensions is that of graviton exchange [81,84,89] in $2 \rightarrow 2$ scattering. This leads to deviations in cross sections and asymmetries in Standard Model processes such as $e^+e^- \rightarrow f\overline{f}$, and may also give rise to new production processes that are not otherwise present at tree-level, such as $e^+e^- \rightarrow hh$, or $\tilde{g}\tilde{g}$. The exchange amplitude is proportional to the sum over the propagators for the graviton KK tower states which, as before, may be converted to an integral over the density of states. However, in this case the integral is divergent for $\delta > 1$ and thus introduces a sensitivity to the unknown ultraviolet physics. Several approaches have been proposed to regulate this integral: (i) a naive cut-off scheme [81,84,89], (ii) an exponential damping due to the brane tension [90], (iii) restrictions from unitarity [91], or (iv) the inclusion of full weakly coupled TeV-scale string theory in the scattering process [92]. Here, we adopt the most model-independent approach, that of a naive cut-off, and set the cut-off equal to $M_*/\lambda^{1/4}$, where λ accounts for the effects of the unknown ultraviolet physics. Assuming that the integral is dominated by the lowest-dimensional local operator, which is dimension-8, this results in a contact-type interaction limit for graviton exchange, which can be described via

$$i\frac{4\lambda}{M_*^4}T^{\mu\nu}T_{\mu\nu}\,, \tag{5.6}$$
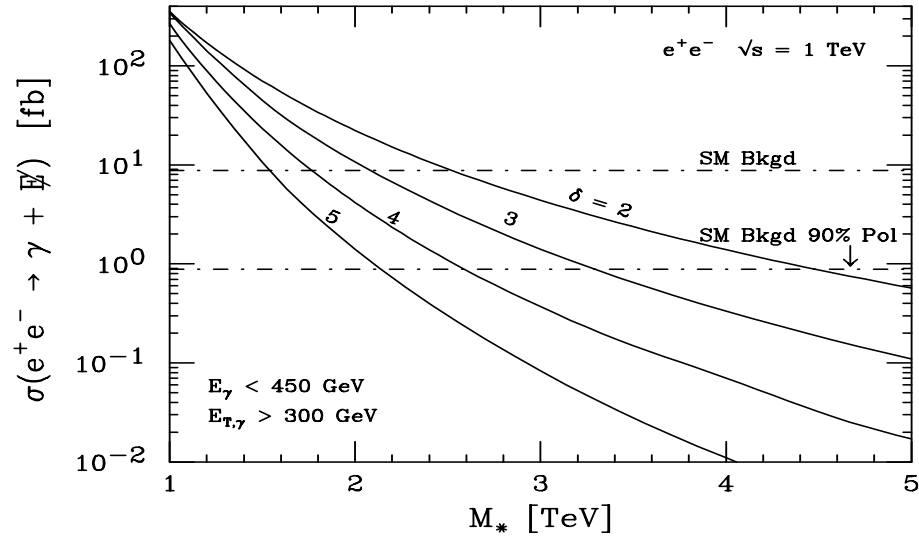
Figure 5.12: The cross section for $e^+e^- \to \gamma G_n$ for $\sqrt{s} = 1$ TeV as a function of the fundamental Planck scale for various values of δ as indicated. The cross sections for the Standard Model background, with and without 90% beam polarization, correspond to the horizontal lines as labeled. The signal and background are computed with the requirement $E_\gamma < 450$ GeV in order to eliminate the $\gamma Z \to \nu \bar{\nu} \gamma$ contribution to the background. From [81].
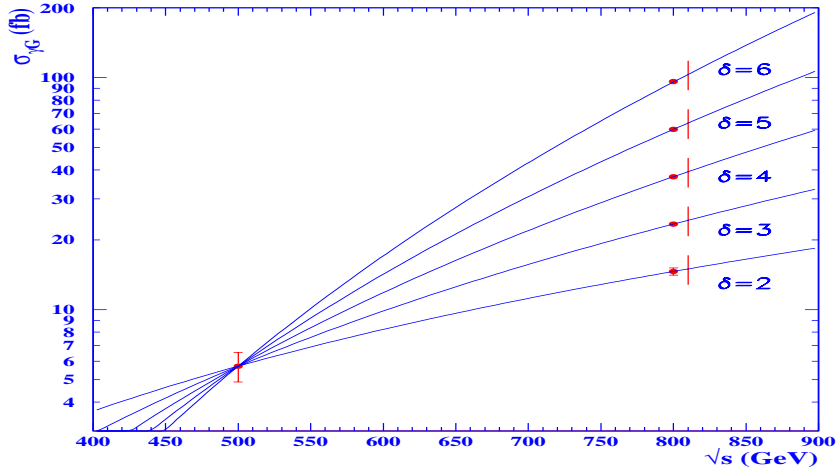
Figure 5.13: The determination of δ from cross section measurements of $e^+e^- \to \gamma G_n$ at $\sqrt{s} = 500$ and 800 GeV with 500 fb^{-1} and 1 ab^{-1}, respectively, taking $P_- = 80\%$ and $P_+ = 60\%$. The 500 GeV cross section has been normalized for the case $M_* = 5$ TeV and $\delta = 2$. From [82].

where $T^{\mu\nu}$ is the stress-energy tensor. This is described in the matrix element for s-channel $2 \to 2$ scattering by the replacement

$$\frac{i^2 \pi}{M_{Pl}^2} \sum_{n=1}^{\infty} \frac{1}{s - m_n^2} \to \frac{\lambda}{M_*^4} \qquad (5.7)$$

with corresponding substitutions for t- and u-channel scattering. Here m_n represents the mass of G_n, the nth graviton KK excitation. This substitution is universal for any $2 \to 2$ process. The resulting angular distributions for fermion pair production are quartic in $\cos\theta$ and thus provide a signal for spin-2 exchange. An illustration of this is given in Fig. 5.14 from [89], which displays the unpolarized angular distribution as well as the angular dependence of the left-right asymmetry in $e^+e^- \to b\bar{b}$, taking $M_* = 3\sqrt{s} = 1.5$ TeV and $\lambda = \pm 1$. The two sets of data points correspond to the two choices of sign for λ, and the error bars represent the statistics in each bin for an integrated luminosity of 75 fb^{-1}. Here, a 60% b-tagging efficiency, 90% electron beam polarization, 10° angular cut, and ISR have been included. The resulting 95% CL search reach with 500 fb^{-1} of integrated luminosity is given in Table 5.6 from summing over the unpolarized and A_{LR} angular distributions for fermion (e, μ, τ, c, b, and t) final states. For comparison, we also present the current bounds [87] from LEP II, HERA, and the DØ Collaboration at the Tevatron, as well as estimates for the LHC with 100 fb^{-1} [89,93] and $\gamma\gamma$ colliders [94]. Note that the $\gamma\gamma \to WW$ process has the highest sensitivity to graviton exchange. This is due to the large W pair cross section and the multitude of observables that can be formed utilizing polarized beams and W decays.

The ability of the LC to determine that a spin-2 exchange has taken place in $e^+e^- \to f\bar{f}$ is demonstrated in Fig. 5.15 from [89]. Here, the confidence level of a fit of spin-2 exchange data to a spin-1 exchange hypothesis is displayed; the quality of such a fit is quite poor almost up to the M_* discovery limit, indicating that the spin-2 nature is discernable.

The scenario with large extra dimensions resolves the hierarchy problem without invoking supersymmetry. However, if this mechanism is embedded in a string theory, then supersymmetry may also be present at the weak scale. A supersymmetric bulk then results in a KK tower of gravitinos, in addition to the KK gravitons. In supersymmetric models that expect a light gravitino, such as gauge-mediated supersymmetry breaking, the gravitino KK tower can yield interesting phenomenological effects. An example of this is in the process $e^+e^- \to \tilde{e}^+\tilde{e}^-$, which would now also receive contributions from t-channel KK gravitino exchange and s-channel KK graviton exchange. This has been studied in [95], which considered an $N = 2$ supersymmetry in the bulk, and after compactifying the gravitino sector, derived the KK gravitino couplings to $N = 1$ supersymmetric matter on the brane. The resulting dramatic effect on selectron pair production is highlighted by the ability to select various production channels via the use of electron beam polarization. This is displayed in Fig.
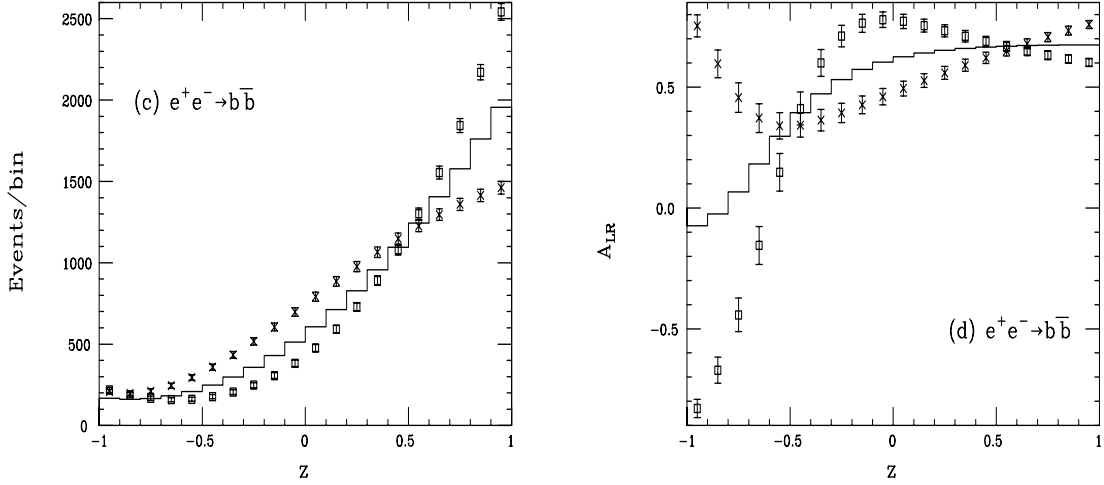
Figure 5.14: Bin-integrated angular distribution and z-dependent ($z = \cos\theta$) left-right asymmetry for $e^+e^- \to b\overline{b}$ at $\sqrt{s} = 500$ GeV. The solid histogram represents the Standard Model while the 'data' points are for $M_* = 1.5$ with $\lambda = \pm 1$. The error bars indicate the statistics in each bin.
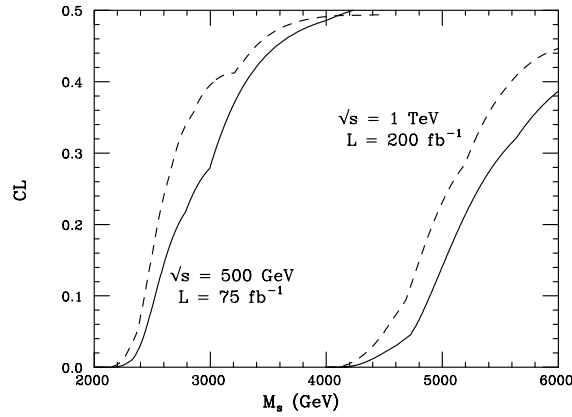
Figure 5.15: The percentage confidence level as a function of M_* for a fit of spin-2 data under a spin-1 hypothesis. The dashed and solid curves correspond to the choice $\lambda = \pm 1$.

		$\sqrt{s}$ (TeV)	M_* (TeV)
LEPII	$e^+e^- \to \ell^+\ell^-, \gamma\gamma, ZZ$	0.2	1.03-1.17
LC	$e^+e^- \to f\overline{f}$	0.5	4.1
LC	$e^+e^- \to f\overline{f}$	1.0	7.2
LC	$\gamma\gamma \to WW$	1.0	13.0
LC	$\gamma\gamma \to \gamma\gamma$	1.0	3.5
LC	$e\gamma \to e\gamma$	1.0	8
HERA	$ep \to e+$ jet	0.314	0.81-0.93
Tevatron Run I	$p\overline{p} \to \ell^+\ell^-, \gamma\gamma$	1.8	1.01-1.08
LHC	$pp \to \ell^+\ell^-$	14.0	7.5
LHC	$pp \to \gamma\gamma$	14.0	7.1

Table 5.6: 95% CL search reach for M_* from graviton exchange in various processes as indicated and discussed in the text. In the bounds from present data, a range is indicated to account for $\lambda = \pm 1$.

5.16, which shows the binned angular distribution for $e^-_{L,R}e^+ \to \tilde{e}^{\mp}_L e^{\pm}_R$ for various values of M_*; this choice of polarization isolates the t-channel neutralino and KK gravitino contributions. The search reach for this process at $\sqrt{s} = 500$ GeV with 80% beam polarization and 500 fb^{-1} of integrated luminosity is $M_* \sim 12$ TeV for the case $\delta = 6$.

6.2   Localized gravity

We now turn to the scenario where the hierarchy is generated by an exponential function of the compactification radius. In its simplest form, gravity propagates in the bulk, while the Standard Model fields are constrained to a 3-brane. This model contains a non-factorizable geometry embedded in a slice of 5-dimensional Anti-de Sitter space (AdS$_5$), which is a space of negative curvature. Two 3-branes reside rigidly at fixed points at the boundaries of the AdS$_5$ slice, located at $|\phi| = 0, \pi$ where ϕ parameterizes the fifth dimension. The 5-dimensional Einstein equations permit a solution that preserves 4-d Poincaré invariance with the metric

$$ds^2 = e^{-2kr_c|\phi|}\eta_{\mu\nu}dx^\mu dx^\nu - r_c^2 d\phi^2 \,, \tag{5.8}$$

where πr_c is the length of the fifth dimenion. The exponential function, or warp factor, multiplying the usual 4-d Minkowski term curves space away from the branes. The constant k is the AdS$_5$ curvature scale, which is of order the Planck scale and is determined by the bulk cosmological constant. The scale of physical phenomena as realized by the 4-d flat metric transverse to the fifth dimension is specified by the exponential warp factor. If the gravitational wavefunction is localized on the brane at $\phi = 0$ (called the 'Planck brane'), then TeV scales can naturally be attained [74]
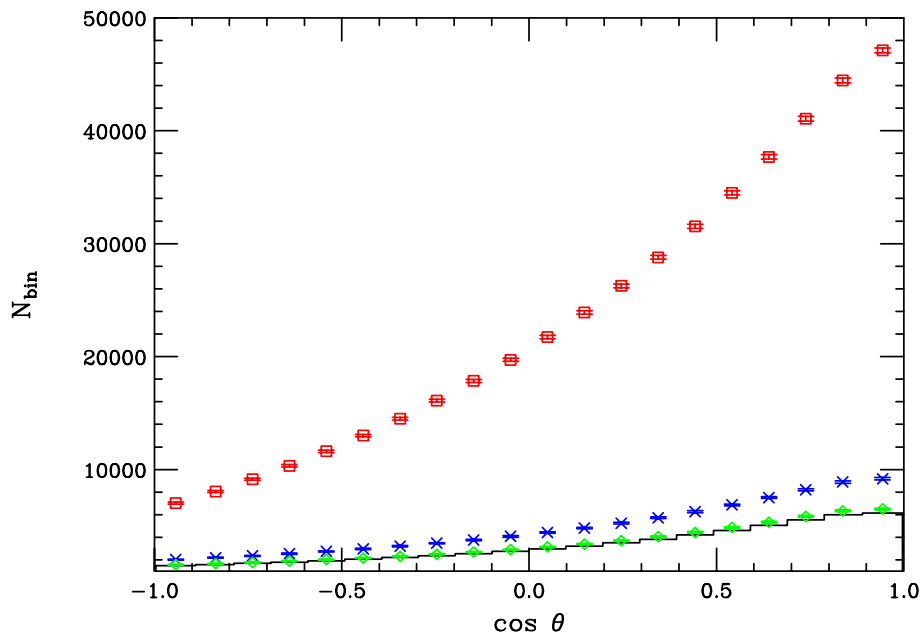
Figure 5.16: The number of events per bin in $e^-_{L,R}e^+ \to \tilde{e}^\mp_L \tilde{e}^\pm_R$ for $\sqrt{s} = 500$ GeV with 500 fb^{-1} of integrated luminosity and $P_- = 80\%$. The curves correspond to $M_* = 1.5, 3, 6$ TeV from top to bottom with the solid histogram representing the minimal supersymmetric case. The error bars correspond to the statistics in each bin. Here the values $m_{\tilde{e}_L} = 220$ GeV and $m_{\tilde{e}_R} = 117$ GeV are assumed.

on the 3-brane at $\phi = \pi$ (the 'TeV brane', where the Standard Model fields reside) if $kr_c \simeq 11$–12. The scale $\Lambda_\pi \equiv \overline{M}_{Pl} e^{-kr_c\pi} \sim 1$ TeV, where $\overline{M}_{Pl} = M_{Pl}/\sqrt{8\pi}$ is the reduced Planck scale, then describes the scale of all physical processes on the TeV-brane. We note that it has been demonstrated [96] that this value of kr_c can be stabilized without fine tuning of parameters.

Two parameters govern the 4-d phenomenology of this model, Λ_π and the ratio $k/\overline{M}_{Pl}$. Constraints on the curvature of the AdS$_5$ space suggest that $k/\overline{M}_{Pl} \lesssim 0.1$. The Feynman rules are obtained by a linear expansion of the flat metric, including the warp factor. After compactification, a KK tower of gravitons appears on the TeV-brane and has masses $m_n = x_n k e^{-kr_c\pi} = x_n \Lambda_\pi k/\overline{M}_{Pl}$ with the x_n being the roots of the first-order Bessel function, i.e., $J_1(x_n) = 0$. Note that the first excitation is naturally of order a few hundred GeV and that the KK states are not evenly spaced. The interactions of the graviton KK tower with the Standard Model fields on the TeV brane are [97]

$$\mathcal{L} = -\frac{1}{\overline{M}_{Pl}} T^{\mu\nu}(x) h^{(0)}_{\mu\nu}(x) - \frac{1}{\Lambda_\pi} T^{\mu\nu}(x) \sum_{n=1}^{\infty} h^{(n)}_{\mu\nu}(x) , \qquad (5.9)$$

where $T^{\mu\nu}$ is the stress-energy tensor. Note that the zero-mode decouples and that the

	$k/\overline{M}_{Pl}$		
	0.01	0.1	1.0
LC $\sqrt{s} = 0.5$ TeV	20.0	5.0	1.5
LC $\sqrt{s} = 1.0$ TeV	40.0	10.0	3.0
LEP II	4.0	1.5	0.4
Tevatron Run II	5.0	1.5	0.5
LHC	20.0	7.0	3.0

Table 5.7: 95% CL search reach for Λ_π in TeV in the contact interaction regime taking 500, 2.5, 2, and 100 fb^{-1} of integrated luminosity at the LC, LEP II, Tevatron, and LHC, respectively. From [97].

couplings of the higher states have inverse-TeV strength. This results in a strikingly different phenomenology from the case of large extra dimensions. Here, the graviton KK tower states are directly produced as single resonances if kinematically allowed.

If the KK gravitons are too massive to be produced directly, their contributions to fermion pair production may still be felt via virtual exchange. In this case, the uncertainties associated with the introduction of a cut-off are avoided, since there is only one additional dimension and the KK states may be neatly summed. The sensitivity [97] to Λ_π at a linear collider for various values of $k/\overline{M}_{Pl}$ is listed in Table 5.7 for 500 fb^{-1} of integrated luminosity. For purposes of comparison, the corresponding reach at LEP II, Tevatron Run II, and the LHC is also displayed.

With sufficient center-of-mass energy the graviton KK states may be produced as resonances. To exhibit how this may appear at a linear collider, Fig. 5.17 displays the cross section for $e^+e^- \to \mu^+\mu^-$ as a function of $\sqrt{s}$, assuming $m_1 = 500$ GeV and taking $k/\overline{M}_{Pl} =$0.01–0.05. The height of the third resonance is somewhat reduced, because the higher KK excitations decay to the lighter graviton states once it is kinematically allowed [98]. In this case one can study graviton self-couplings, and higher-energy e^+e^- colliders may become graviton factories!

Searches for the first graviton KK resonance in Drell-Yan and di-jet data at the Tevatron already place non-trivial restrictions [97] on the parameter space of this model, given roughly by $m_1 \gtrsim 175, 550, 1100$ GeV for $k/\overline{M}_{Pl} = 0.01, 0.1, 1.0$. Precision electroweak data extend [99] this search reach for smaller values of k. These constraints, taken together with the theoretical prejudices that (i) $\Lambda_\pi \lesssim 10$ TeV, $i.e.$, the scale of physics on the TeV brane is not far above the electroweak scale and (ii) $k/\overline{M}_{Pl} \lesssim 0.1$ from the above-mentioned AdS$_5$ curvature considerations, result in a closed allowed region in the 2-dimensional parameter space, which can be completely explored at the LHC [99,100] via the Drell-Yan mechanism.

Lastly, we note that if the Standard Model fields are also allowed to propagate in the bulk [99,101], the phenomenology can be markedly different, and is highly dependent on the value of the 5-dimensional fermion mass. For various phenomenological
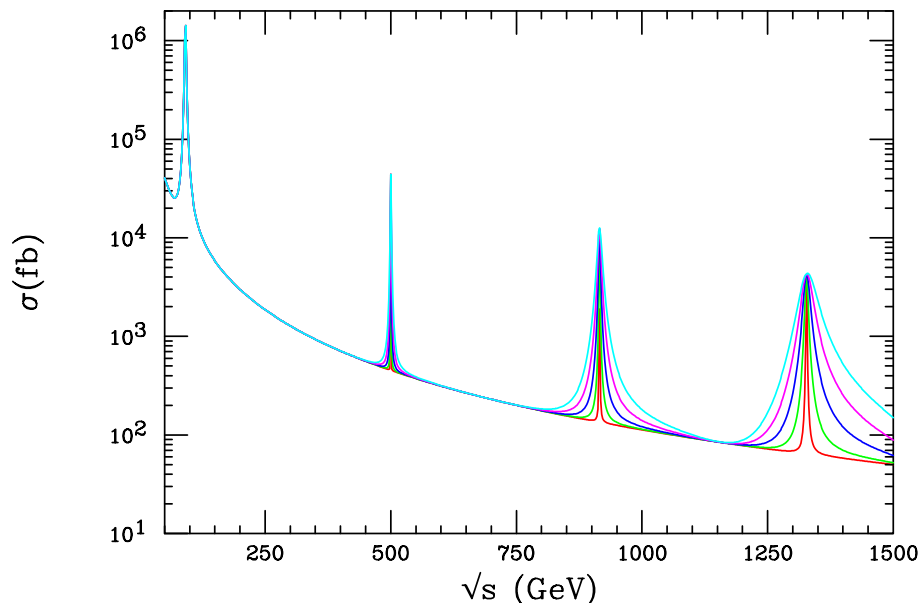
Figure 5.17: The cross section for $e^+e^- \to \mu^+\mu^-$ including the exchange of a KK tower of gravitons with $m_1 = 500$ GeV. The curves correspond to $k/\overline{m}_{Pl} =$ in the range 0.01–0.05.

reasons, it is least problematic to keep the Higgs field on the TeV brane [101]. As a first step, one can study the effect of placing the Standard Model gauge fields in the bulk and keeping the fermions on the TeV-brane. In this case, the fermions on the wall couple to the KK gauge fields a factor of $\sqrt{2kr_c\pi} \sim 9$ times more strongly than they couple to the $(\gamma, g, W^\pm, Z)$. In this case, precision electroweak data place strong constraints, requiring that the lightest KK gauge boson have a mass greater than about 25 TeV. This value pushes the scale on the TeV-brane above 100 TeV, making this scenario disfavored in the context of the hierarchy problem.

This bound can be relaxed if the fermions also reside in the bulk [101]. By introducing bulk fermion 5-d masses m_5, the couplings of the fermion zero modes (*i.e.*, the Standard Model fermions) to various KK fields become a function of the bulk mass parameter $\nu \equiv m_5/k$. The parameter ν controls the shape of the fermion zero-mode wavefunction, with negative (positive) values of ν serving to localize the wavefunction near the Planck brane (TeV brane). Constraints from avoiding flavor-changing neutral currents, Yukawa coupling blow-up, and the generation of a new hierarchy result in a rather narrow allowed range of ν. For some values of ν in this range, the fermionic couplings of the KK graviton states essentially vanish, and hence the graviton production mechanisms discussed above are no longer viable. In this case, the gravitons retain a small coupling to the Standard Model gauge bosons, and the most promising production mechanism [99] is at a photon collider via $\gamma\gamma \to G_n \to hh$, with h being the Higgs boson.

221

6.3 TeV-scale extra dimensions

TeV^{-1}-sized extra dimensions can naturally arise in some string theory models [75], and in this case, the Standard Model fields may feel their effects. The physics of models with KK excitations of the Standard Model gauge bosons arising from TeV-scale extra dimensions has been discussed for some time [102]. The various models in this class of theories differ in detail in two regards: (i) the placement of the Higgs field(s) in the bulk or on the wall(s), and (ii) the treatment of the fermion fields.

If Higgs fields propagate in the bulk, the expectation value of the zero-mode field generates electroweak symmetry breaking. In this case, there is no mixing among the various gauge boson KK modes. Thus the KK mass matrix is diagonal, with the masses of the excitations given by $[M_0^2 + \vec{n} \cdot \vec{n} M_c^2]^{1/2}$, where M_0 is the zero-mode mass, M_c is the compactification mass scale and $\vec{n}$ is a set of integers labeling the excitation state. However, if the Higgs is a wall field, its expectation value induces off-diagonal elements in the mass matrix and thus a mixing among the gauge KK states. In this case the mass matrix needs to be diagonalized to determine the masses and couplings of the gauge KK states. It is also possible to imagine a more generalized mixed scenario with two Higgs fields, one residing in the bulk and one on the wall, that share the SM symmetry breaking. Clearly, the detailed phenomenology of these possibilities will be quite different. For example, a small mixing of the gauge KK states may show up in precision measurements when W and Z properties are compared with Standard Model expectations.

An even more diverse situation arises when one considers the placement of the Standard Model fermions within the extra dimensions. There are essentially three possibilities:

(a) The fermions are constrained to 3-branes located at fixed points. This is the most common situation discussed in the literature [83] and in this case the fermions are not directly affected by the extra dimensions. For models in this class, global fits to precision electroweak data place strong lower bounds on the value of M_c, which corresponds to the mass of the first gauge KK excitation. Following the analysis of Rizzo and Wells [83] and employing the most recent data [103], one finds that $M_c > 4.4$ TeV when the Higgs field is on the wall; the bound is 4.6 TeV when the Higgs field is in the bulk. Such a large mass for gauge KK states is beyond the direct reach of a LC, but the KK states can be directly produced as resonances at the LHC in the Drell-Yan channel provided that $M_c \lesssim 6$ TeV. This reach at the LHC may be extended by a TeV or so [104] by examination of the Drell-Yan line shape at high lepton-pair invariant mass. However, the LC can indirectly observe the existence of heavy gauge KK states via their s-channel exchanges in the contact interaction limit. Combining the results from various fermion final states in $e^+e^- \to f\overline{f}$ gives the 95% CL search reach displayed in Table 5.8.

If a $\gamma^{(1)}/Z^{(1)}$ KK resonance is observed at the LHC, a $\sqrt{s} = 500$ GeV linear

	M_c Reach (TeV)
Tevatron Run II 2 fb^{-1}	1.1
LHC 100 fb^{-1}	6.3 ($\sim$ 7.5)
LEP II	3.1
LC $\sqrt{s} = 0.5$ TeV 500 fb^{-1}	13.0
LC $\sqrt{s} = 1.0$ TeV 500 fb^{-1}	23.0
LC $\sqrt{s} = 1.5$ TeV 500 fb^{-1}	31.0

Table 5.8: 95% CL search reach for the mass of the first KK gauge boson excitation. From Rizzo and Wells [83]. The LHC reach is via direct observation of a resonance, while the LC sensitivities are from indirect effects as in the case of a search for a new neutral gauge boson. The number in parentheses for the LHC is an estimate of the extension of the complete search reach including indirect effects from contact interactions.

collider can distinguish this state from a new neutral gauge boson arising from an extended gauge sector by using the Bhabha scattering channel. If one attempts to fit the induced deviations in the Bhabha cross section and polarized asymmetry by varying the vector and axial-vector couplings of a hypothetical non-KK Z', one finds [105] that the CL of the fit is quite poor ($\lesssim 10^{-3}$). This demonstrates that the assumption that the KK state is a Z' is incorrect. A separate fit assuming that the resonance is a KK state yields a good fit. At the LHC, it is currently unclear whether the $\gamma^{(1)}/Z^{(1)}$ KK resonance can be distinguished from a Z' in a model-independent manner.

(b) The Standard Model fermions are localized at specific points, x_i, in the extra TeV dimension, which are not necessarily at the orbifold fixed points. Here, the zero- and excited-mode fermions obtain narrow Gaussian-like wave functions in the extra dimensions with a width σ much smaller than the compactification scale, i.e., $(\sigma/\pi r_c)^2 \ll 1$. The placement of SM fermions at different locations and the narrowness of their wavefunctions can then suppress [76] the rates for a number of dangerous processes such as proton decay. For the lighter gauge KK modes (small values of n), the width of the fermion wavefunction centered at a given point cannot be resolved, so that the wavefunction appears similar to a delta function. Thus the coupling of the fermion to these gauge KK states is determined by the value of the gauge KK wavefunction evaluated at that point. However, when $n\sigma/\pi r_c$ grows to order unity or larger, the KK gauge field can resolve the finite size of the fermion wavefunction and the coupling of the fermion becomes exponentially damped. This decouples the heavy gauge KK states, providing a means of rendering sums over KK towers of gauge bosons finite in the case of two or more extra dimensions [106]. An analysis of precision electroweak data in this case shows that M_c is typically found to be $\geq 3 - 4$ TeV. Depending upon the properties of the compactification manifold, measurements at colliders may probe the distance in the extra dimensions between two fermions,

$|x_i - x_j|$, in $2 \to 2$ scattering. For example, in this case Bhabha scattering can probe the distance between the left- and right-handed electrons, as illustrated in Fig. 5.18. A study of the cartography of the localized fermions at linear colliders has been performed in [107]. At very large energies, the cross section for the polarized version of this process will tend rapidly to zero since the two particles completely miss each other in the extra dimension [108].

(c) The fermions are fields in the bulk. This possibility is known as the 'universal extra dimensions' scenario [109]. This case is different in that walls or branes are not present and hence momentum is conserved in the additional dimensions. The consequence of this is that KK number is conserved at all interaction vertices, hence only pairs of KK gauge bosons couple to the zero-mode fermions. In this case, electroweak precision data as well as direct searches for KK states lead to a reduced lower bound of $M_c \simeq 0.4$ TeV. Without further ingredients, this model may have trouble satisfying cosmological constraints, since the lightest KK excitations are absolutely stable. This may be avoided if there is any small breaking of translation invariance in the extra dimensions. Alternatively, one can imagine the gauge and fermion KK
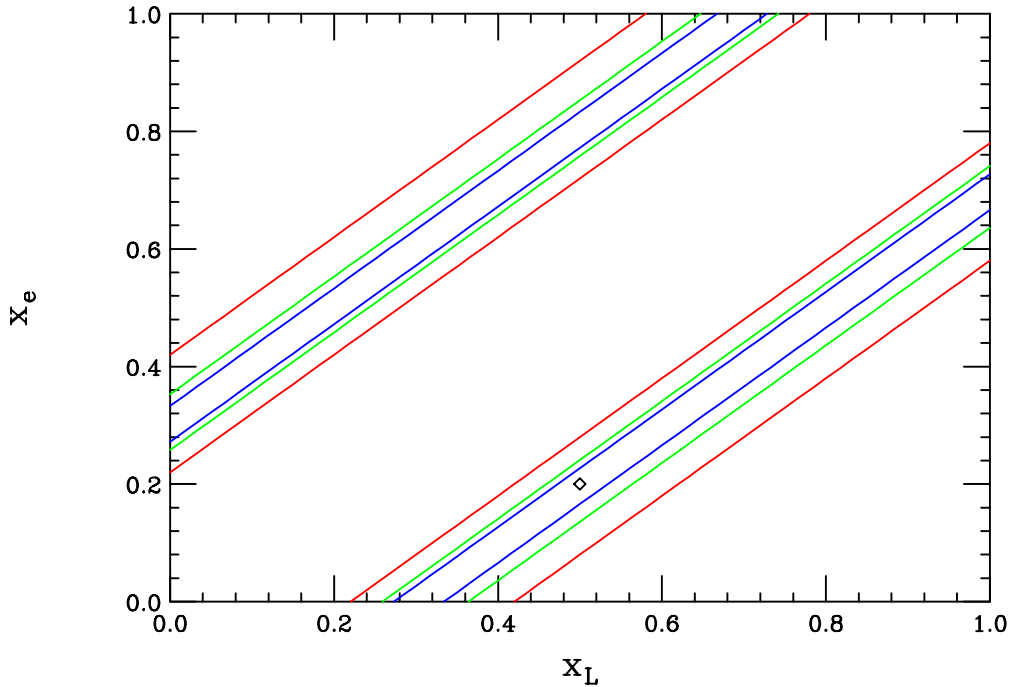
Figure 5.18: The ability of a LC to determine the separation in the extra dimension of right- and left-handed electrons from Bhabha scattering. The red, green, and blue (outer, middle, and inner) set of curves correspond to $\sqrt{s} = 500$, 1000, 1500 GeV, respectively, with 500 fb^{-1} assumed for each energy. This case assumes $M_c = 4$ TeV and that the location of the right- (left-)handed electron, $x_{e(L)}$, is given by a Gaussian centered at 0.2 (0.5) $\cdot 2\pi r_c$.

fields as confined to a brane of thickness TeV^{-1}, *i.e.*, a thick brane, embedded in a highe-dimensional space that includes gravity. In this case the higher-level KK modes can decay down to the zero modes via graviton emission, but at a rate determined by the 'form factor' of the brane [110]. In either case an interesting phenomenology results. The KK states are produced in pairs at colliders and then either decay via one of these two mechanisms or are long-lived and appear as tracks in a detector.

7 Highly non-conventional theories and possible surprises

So far in this chapter, we have delineated the potential of a linear collider to explore the new physics that is present in set classes of established models. However, as likely as not, when Nature finally reveals her mysteries they will be full of surprises that lie outside the realm of our limited imaginations.

Along these lines, we note that some of the most striking recent developments have occured in string theory. While it is currently difficult to relate these theories to experiment, some of their ingredients, when considered on their own, have interesting phenomenological consequences. Here, we consider two such examples of this top-down approach, as a demonstration of the potential of the LC to discover the unforseen.

7.1 String resonances

If the scenario with large extra dimensions discussed in a previous section is embedded in a string theory, then stringy effects must also appear at the TeV scale. Hence, not only the gravitons, but also the Standard Model fields must have an extended structure. The exchange of string Regge excitations of Standard Model particles in $2 \rightarrow 2$ scattering may appear as contact-like interactions with a strength that overwhelms the corresponding graviton exchange. This is deduced from simple coupling-counting arguments. Yang-Mills bosons live at the end of open strings, while gravitons correspond to closed string states, which require an additional coupling constant factor at the amplitude level. Hence the exchange of KK graviton states is suppressed by a factor of g^2 compared to the exchange of string Regge excitations.

This has been examined in [111], where an illustrative string model was assumed. This model makes use of scattering amplitudes on the 3-brane of weakly coupled type IIB string theory to describe a string version of QED. Electrons and photons then correspond to massless states of open strings ending on the 3-brane and are characterized by the quantum theory of fluctuations of an open string with specified boundary conditions. Within the context of this model, Bhabha scattering and pair annihilation receive contributions from the string Regge exchanges. The differential

cross section for these processes is modified by a form factor,

$$\frac{d\sigma}{d\cos\theta} = \left(\frac{d\sigma}{d\cos\theta}\right)_{SM} \left|\frac{\Gamma(1-s/M_{str}^2)\Gamma(1-t/M_{str}^2)}{\Gamma(1-s/M_{str}^2-t/M_{str}^2)}\right|^2 , \tag{5.10}$$

which essentially mirrors the original Veneziano result [112]. Here, M_{str} represents the string scale and can be related to the fundamental Planck scale in the large extra dimension scenario via $M_*/M_{str} = \pi^{-1/8}\alpha^{-1/4}$. Figure 5.19 displays the deviation from Standard Model expectations to Bhabha scattering from these string exchanges, and compares their effect to those arising from other types of contact interactions. The 95% CL exclusion limits for $\sqrt{s} = 1$ TeV and 200 fb^{-1} is $M_{str} > 3.1$ TeV, which corresponds to $M_*/\lambda^{1/4} > 9.3$ TeV.
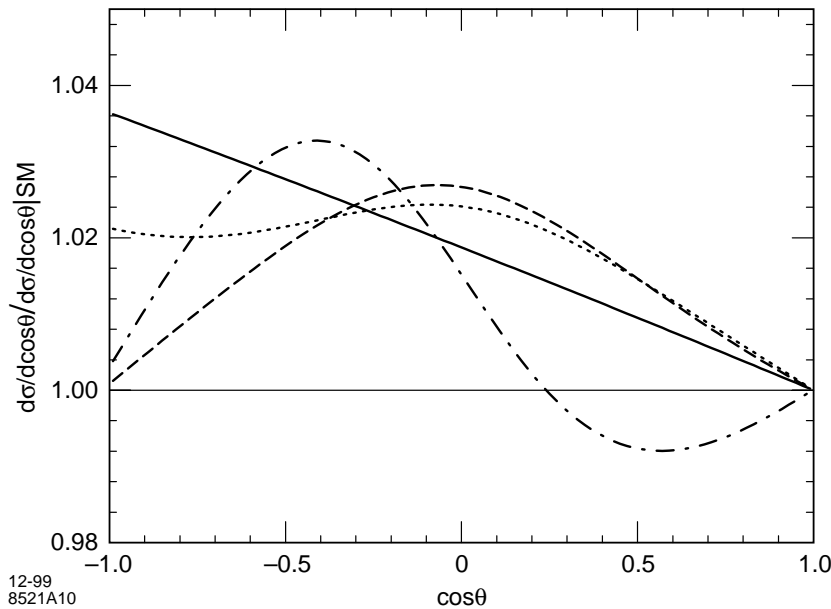
Figure 5.19: Comparison of deviations from the Standard Model prediction for Bhabha scattering at 1 TeV due to corrections from higher-dimension operators [111]. The curves correspond to: string model with $M_{str} = 3.1$ TeV (solid), KK graviton exchange with $M_*/\lambda^{1/4} = 6.2$ TeV (dotted), VV contact interactions with $\Lambda = 88$ TeV (dashed), and AA contact interactions with $\Lambda = 62$ TeV (dot-dashed).

7.2 Non-commutative field theories

Recent theoretical results have demonstrated that non-commutative quantum field theories (NCQFT) naturally appear within the context of string theory and M-theory [113]. In this case, the usual δ-dimensional space associated with commuting space-time coordinates is generalized to one that is non-commuting. In such

a space, the conventional coordinates are represented by operators that no longer commute,

$$[\hat{X}_\mu, \hat{X}_\nu] = i\theta_{\mu\nu} \equiv \frac{i}{\Lambda^2_{NC}} c_{\mu\nu} \,. \tag{5.11}$$

Here, the effect has been parameterized in terms of an overall scale Λ_{NC}, which characterizes the threshold where non-commutative (NC) effects become important, and a real antisymmetric matrix $c_{\mu\nu}$, whose dimensionless elements are presumably of order unity. The most likely value of Λ_{NC} is near the string scale or the true Planck scale, which could be as low as the TeV scale. The matrix $c_{\mu\nu}$ is related to the Maxwell field-strength tensor $F_{\mu\nu}$ in a straightforward fashion, since NCQFT arises in string theory in the presence of background electromagnetic fields. The matrix $c_{\mu\nu}$ is identical in all reference frames, defining a preferred NC direction in space, and hence Lorentz invariance is violated at energies of order Λ_{NC}. The usual description of Lorentz violation needs to be modified in order to apply to NCQFT; present experiments only constrain such effects at the few-TeV level [114].

Caution must be exercised to preserve orderings of the products of fields when formulating NCQFT. This is accomplished with the introduction of the star product, $\phi(\hat{X})\phi(\hat{X}) = \phi(x) * \phi(x) = \phi(x)e^{[i\theta^{\mu\nu}\partial_\mu\partial_\nu/2]}\phi(x)$, which absorbs the effect of the commutation relation via a series of Fourier transforms. The NC action for a quantum field theory is thus obtained from the ordinary one by replacing the products of fields by star products. A striking consequence of this is that the NC version of QED takes on a non-Abelian nature in that both 3-point and 4-point photon couplings are generated. In addition, all QED vertices pick up additional phase factors that are dependent upon the momenta flowing through the vertex. We note that propagators, however, are not modified since quadratic forms remain unchanged under the properties of the star product. NC effects thus produce striking signatures in QED processes at a linear collider. The modifications to pair annihilation, Bhabha and Møller scattering, as well as $\gamma\gamma \rightarrow \gamma\gamma$ have been studied in [115]. Pair annihilation and $\gamma\gamma$ scattering both receive new diagrammatic contributions due to the non-Abelian couplings, and all four processes acquire a phase dependence due to the relative interference of the vertex kinematic phases. The lowest-order correction to the Standard Model in these processes occurs at dimension 8. The most striking result is that a ϕ dependence is induced in $2 \rightarrow 2$ scattering processes because of the existence of the NC preferred direction in space-time. This azimuthal dependence in pair annihilation is illustrated in Fig. 5.20 for the case where the NC direction is perpendicular to the beam axis. The results of [115] are summarized in Table 5.9, which displays the 95% CL search reach for the NC scale in these four reactions. We see that these processes are complementary in their ability to probe different structures of non-commuting space-time.
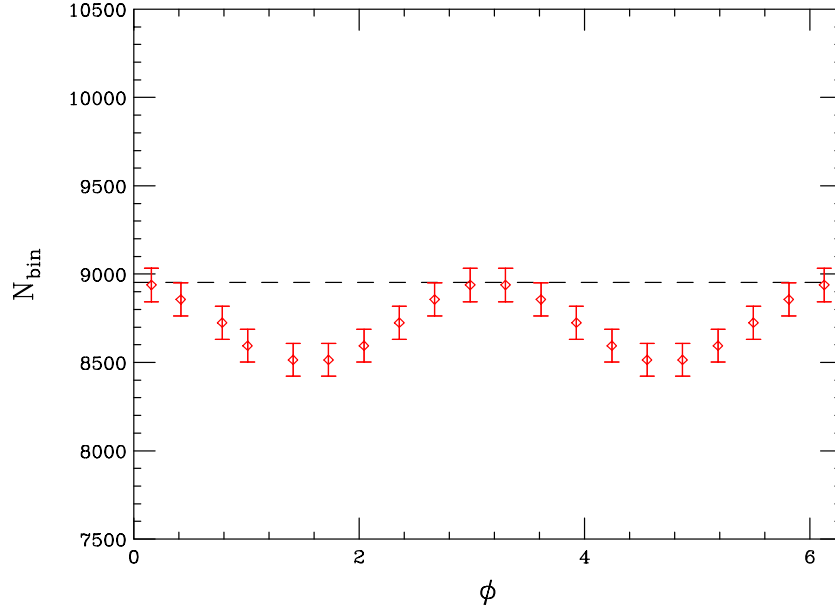
Figure 5.20: ϕ dependence of the $e^+e^- \to \gamma\gamma$ cross section, taking $\Lambda_{NC} = \sqrt{s} = 500$ GeV a luminosity of $500\,\text{fb}^{-1}$. A cut of $|\cos\theta| < 0.5$ has been employed. The dashed line corresponds to the SM expectations and the 'data' points represent the NCQED results.

Process	Structure Probed	Bound on Λ_{NC}
$e^+e^- \to \gamma\gamma$	Space-Time	$740 - 840$ GeV
Møller Scattering	Space-Space	1700 GeV
Bhabha Scattering	Space-Time	1050 GeV
$\gamma\gamma \to \gamma\gamma$	Space-Time	$700 - 800$ GeV
	Space-Space	500 GeV

Table 5.9: Summary of the 95% CL search limits on the NC scale Λ_{NC} from the various processes considered above at a 500 GeV linear collider with an integrated luminosity of $500\,\text{fb}^{-1}$.

8   Determining the origin of new physics

As demonstrated in this chapter, some reactions at linear colliders may receive contributions from many different models. An example of this is $e^+e^- \to f\overline{f}$, in which indirect effects of compositeness, extended gauge sectors, extra dimensions, string resonances, or supersymmetry may be revealed. Once a signal for new physics is found, the next step is to unravel the properties associated with the new phenomena. If the mass spectrum of the new particles in these theories is kinematically accessible, then their properties may be directly measured. However, if these states are too heavy, then we must explore their characteristics indirectly. This is feasible at a linear

collider because of the precision at which measurements can be performed. Here, we give a single example to illustrate our point, namely, the ability of e^+e^- colliders to provide unique information about the spin structure of new objects. The angular distributions and polarization asymmetries associated with $e^+e^- \to f\overline{f}$ are sensitive probes of the spin of new particles. An illustration of this was presented in Fig. 5.15, which showed the extent to which spin-2 exchange in $e^+e^- \to f\overline{f}$ is distinguishable from other new physics sources. This figure showed that deviations induced by spin-2 graviton exchanges can be distinguished from those due to lower spins, such as new vector bosons Z' or a scalar neutrino in R-parity-violating models, up to the discovery limit. In addition, discrimination between spin-1 and spin-0 particles at a LC was demonstrated [116] by studying the angular distributions induced by the exchange of a Z' and of a scalar neutrino, $\tilde{\nu}$ in $e^+e^- \to f\overline{f}$. A two-parameter fit of a trial distribution of the form $\sim A(1+z)^2 + B(1-z)^2$ was performed to the observables, with A, B being parameters determined by the fit. In the case of the Standard Model and Z', the fitted parameters A, B are constant, while, in the case of $\tilde{\nu}$, the parameter B depends on z. The results of the fit are displayed in Fig. 5.21. The Standard Model values of A and B are shown in the center of the figure and are assumed to be known precisely. The Z' mass was set to 3 TeV and four different Z' coupling values were considered. The $\tilde{\nu}$ was allowed to mediate the reaction in both s- and t-channels. All
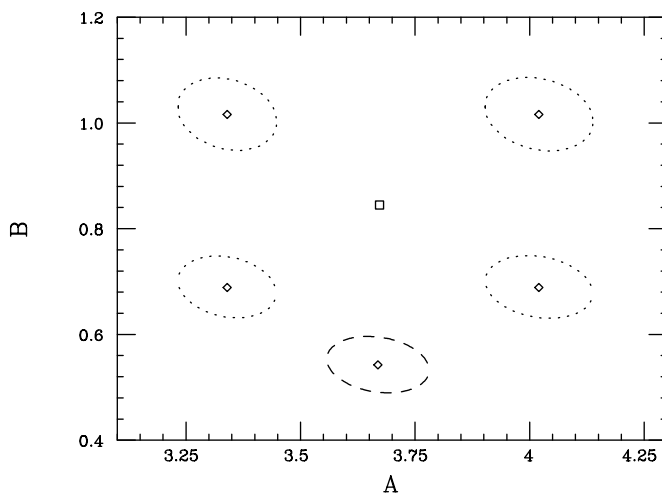
Figure 5.21: Results of the fit with 95% CL contours circled around the fitted values. The box in the center corresponds to the Standard Model, the dotted ellipses represent the fit to the four Z' cases considered, and the dashed ellipse is for the case of sneutrino exchange. The fit was performed taking $\sqrt{s} = 1$ TeV with 150 fb^{-1}.

five regions are statistically well separated from each other, and clearly distant from the Standard Model solution.

9   Conclusions

In this chapter, we have discussed several classes of motivated models that contain new phenomena, and we have delineated the ability of a linear collider to explore them. We have seen that the LHC and the linear collider have a comparable and complementary discovery potential. In many cases, a signal for new physics will first be observed at the LHC, and the linear collider will precisely determine its properties. While a 500 GeV linear collider has a large discovery reach and potential to elucidate the underlying physics, every physics scenario we have also explored benefits from an upgrade to higher energy.

However, our limited imagination does not span the full range of alternatives allowed by present data. We thus must be prepared to discover the unexpected, which is best accomplished by exploration of the energy frontier by both e^+e^- and hadron colliders.

References

[1] K. Hagiwara, R. D. Peccei, D. Zeppenfeld and K. Hikasa, Nucl. Phys. **B282**, 253 (1987).

[2] J. Bagger, S. Dawson, and G. Valencia, Nucl. Phys. **B399**, 264 (1993).

[3] C. Ahn, M. E. Peskin, B. W. Lynn and S. B. Selipsky, Nucl. Phys. **B309**, 221 (1988); J. Fleischer, J. L. Kneur, K. Kolodziej, M. Kuroda and D. Schildknecht, Nucl. Phys. **B378**, 443 (1992) [Erratum-ibid. **B426**, 443 (1992)].

[4] A. Arhrib, J. L. Kneur and G. Moultaka, Phys. Lett. **B376**, 127 (1996); E. N. Argyres, A. B. Lahanas, C. G. Papadopoulos and V. C. Spanos, Phys. Lett. **B383**, 63 (1996); G. Couture, J. N. Ng, J. L. Hewett, and T. G. Rizzo, Phys. Rev. **D38**, 860 (1988).

[5] M. Kitahara, M. Marui, N. Oshimo, T. Saito and A. Sugamoto, Eur. Phys. J. **C4**, 661 (1998), [hep-ph/9710220].

[6] C. Burgard, in *Physics and Experiments with Future e^+e^- Linear Colliders*, E. Fernández and A. Pacheco, eds. (UAB Publications, Barcelona, 2000); W. Menges, "A Study of Charge Current Triple Gauge Couplings at TESLA." LC-PHSM-2001-022. `http://www.desy.de/~lcnotes`.

[7] D. Choudhury, J. Kalinowski, Nucl. Phys. **B491**, 129 (1997); D. Choudhury, J. Kalinowski, A. Kulesza, Phys. Lett. **B457**, 193 (1999).

[8] ATLAS Detector and Physics Performance Technical Design Report, LHCC 99-14/15 (1999).

[9] A. Vicini, Acta Phys. Polon. **B29**, 2847 (1998).

[10] M. W. Grünewald *et al.*, in *Reports of the Working Groups on Precision Calculations for LEP2 Physics*, S. Jadach, G. Passarino, and R. Pittau, eds. (CERN 2000-009, Geneva, 2000) [hep-ph/0005309].

[11] W. Beenakker, F. A. Berends and A. P. Chapovsky, Nucl. Phys. **B548**, 3 (1999).

[12] A. Denner, S. Dittmaier, M. Roth and D. Wackeroth, Nucl. Phys. **B587**, 67 (2000); Phys. Lett. **B475**, 127 (2000).

[13] S. Jadach, W. Placzek, M. Skrzypek, B. F. Ward and Z. Was, Phys. Lett. **B417**, 326 (1998); Phys. Rev. **D61**, 113010 (2000); hep-ph/0007012; hep-ph/0103163; hep-ph/0104049.

[14] Y. Kurihara, M. Kuroda and D. Schildknecht, Nucl. Phys. **B565**, 49 (2000).

[15] A. Denner, S. Dittmaier, M. Roth and D. Wackeroth, hep-ph/0104057; A. Denner, S. Dittmaier, M. Roth and D. Wackeroth, in *Proceedings of the 22nd Annual MRST Meeting*, C.R. Hagen, ed. (Melville, NY, 2000) [hep-ph/0007245].

[16] W. J. Stirling and A. Werthenbach, Phys. Lett. **B466**, 369 (1999); Eur. Phys. J. **C14**, 103 (2000).

[17] G. Belanger, F. Boudjema, Y. Kurihara, D. Perret-Gallix and A. Semenov, Eur. Phys. J. **C13**, 283 (2000).

[18] P. J. Dervan, A. Signer, W. J. Stirling and A. Werthenbach, J. Phys. **G26**, 607 (2000).

[19] G. Montagna, M. Moretti, O. Nicrosini, M. Osmo and F. Piccinini, hep-ph/0103155.

[20] The LEP Collaborations ALEPH, DELPHI, L3, OPAL, the LEP Electroweak Working Group, and the SLD Heavy and Flavor and Electroweak Groups, CERN-EP/2001-021, hep-ex/0103048.

[21] G. Belanger and F. Boudjema, Phys. Lett. **B288**, 201 (1992). F. Boudjema *et al.*, in *Proceedings of the workshop on e^+e^- collisions at 500 GeV*, P. Zerwas, ed. (Munich/Annecy/Hamburg, 1991), ENSLAPP-A-365-92. S. Godfrey, in *Proceedings of the International Symposium On Vector Boson Self-interactions*, U. Baur, S. Errede, T. Muller, eds. (Woodbury, NY, American Inst. Phys., 1996) [hep-ph/9505252].

[22] G. Abu Leil and W. J. Stirling, J. Phys. **G21**, 517 (1995).

[23] S. Dawson, A. Likhoded, G. Valencia and O. Yushchenko, in *Proceedings of the 1996 DPF/DPB Summer Study On New Directions For High-Energy Physics* (Snowmass 96), D. G. Cassel, L. T. Gennari, R. H. Siemann, eds. (Stanford, CA, 1997) [hep-ph/9610299]; T. Han, H. He and C. P. Yuan, Phys. Lett. **B422**,

294 (1998); O. J. Eboli, M. C. Gonzalez-Garcia and J. K. Mizukoshi, Phys. Rev. **D58**, 034008 (1998) [hep-ph/9711499]; F. Gangemi, hep-ph/0002142.

[24] A. S. Belyaev, O. J. Eboli, M. C. Gonzalez-Garcia, J. K. Mizukoshi, S. F. Novaes and I. Zacharov, Phys. Rev. **D59**, 015022 (1999); S. Haywood *et al.*, in *Proceedings of the CERN-TH workshop on Standard Model Physics (and more) at the LHC*, G. Altarelli and M. Mangano, eds. (Geneva, CERN, 2000); W. J. Stirling and A. Werthenbach, Eur. Phys. J. **C12**, 441 (2000).

[25] O. J. Eboli, M. C. Gonzalez-Garcia, S. M. Lietti and S. F. Novaes, Phys. Rev. **D63**, 075008 (2001); O. J. Eboli, M. C. Gonzalez-Garcia and S. F. Novaes, Nucl. Phys. **B411**, 381 (1994) [hep-ph/9306306].

[26] M. E. Peskin and J. D. Wells, hep-ph/0101342.

[27] For recent reviews, see K. Lane, "Technicolor 2000," hep-ph/0007304; R. S. Chivukula and J. Womersley, in "Review of Particle Physics," D. E. Groom *et al.*, Eur. Phys. J. **C15**, 1 (2000).

[28] T. Appelquist, J. Terning and L. C. Wijewardhana, Phys. Rev. Lett. **79**, 2767 (1997).

[29] R. Casalbuoni, A. Deandrea, S. De Curtis, D. Dominici, R. Gatto and J. F. Gunion, Nucl. Phys. **B555**, 3 (1999).

[30] C. T. Hill, Phys. Lett. **B345**, 483 (1995); K. Lane and E. Eichten, Phys. Lett. **B352**, 382 (1995) [hep-ph/9503433].

[31] C. Yue, G. Lu, J. Cao, J. Li and G. Liu, Phys. Lett. **B496**, 93 (2000).

[32] T. L. Barklow *et al.*, in *Proceedings of the 1996 DPF/DPB Summer Study On New Directions For High-Energy Physics* (Snowmass 96), D. G. Cassel, L. T. Gennari, and R. H. Siemann, eds. (SLAC,1997) [hep-ph/9704217].

[33] V. Barger, K. Cheung, T. Han and R. J. Phillips, Phys. Rev. **D52**, 3815 (1995); E. Boos, H. J. He, W. Kilian, A. Pukhov, C. P. Yuan and P. M. Zerwas, Phys. Rev. **D57**, 1553 (1998); Phys. Rev. **D61**, 077901 (2000).

[34] R. Chierici, S. Rosati, M. Kobel, "Strong electroweak symmetry breaking signals in WW scattering at TESLA," LC-PHSM-2001-038, http://www.desy.de/~lcnotes.

[35] T. L. Barklow, in *Proceedings of the 1996 DPF/DPB Summer Study On New Directions For High-Energy Physics* (Snowmass 96), D. G. Cassel, L. T. Gennari, and R. H. Siemann, eds. (SLAC,1997); E. Ruiz Morales and M. E. Peskin, hep-ph/9909383; T. Han, Y. J. Kim, A. Likhoded and G. Valencia, Nucl. Phys. **B593**, 415 (2001); F. Larios, T. M. Tait and C. P. Yuan, hep-ph/0101253.

[36] A. Manohar and H. Georgi, Nucl. Phys. B **234**, 189 (1984).

[37] M. Peskin, in *Physics in Collision IV*, A. Seiden, ed. (Éditions Frontières, Gif-Sur-Yvette, France, 1984); F. Iddir, A. Le Yaouanc, L. Oliver, O. Pene and J. C. Raynal, Phys. Rev. **D41**, 22 (1990).

[38] T. L. Barklow, "LET Signals in $e^+e^- \rightarrow W^+W^-$ at $\sqrt{s} = 800$ GeV" in *Proceedings of 5th International Linear Collider Workshop* (LCWS2000).

[39] C. J. S. Damerell and D. J. Jackson, in *Proceedings of the 1996 DPF/DPB Summer Study On New Directions For High-Energy Physics* (Snowmass 96), D. G. Cassel, L. T. Gennari, and R. H. Siemann, eds. (SLAC,1997).

[40] B. A. Dobrescu and C. T. Hill, Phys. Rev. Lett. **81**, 2634 (1998); R. S. Chivukula, B. A. Dobrescu, H. Georgi and C. T. Hill, Phys. Rev. **D59**, 075003 (1999).

[41] C. T. Hill, Phys. Lett. **B266**, 419 (1991).

[42] G. Burdman and N. Evans, Phys. Rev. **D59**, 115005 (1999).

[43] R. S. Chivukula, C. Hölbling and N. Evans, Phys. Rev. Lett. **85**, 511 (2000).

[44] B. A. Dobrescu, Phys. Rev. **D63**, 015004 (2001).

[45] B. A. Dobrescu, G. Landsberg and K. T. Matchev, Phys. Rev. **D63**, 075003 (2001)

[46] P. F. Derwent *et al.*, "Linear Collider Physics", FERMILAB-FN-701, (2000).

[47] H. Collins, A. Grant and H. Georgi, Phys. Rev. **D61**, 055002 (2000).

[48] H. Georgi and A. K. Grant, Phys. Rev. **D63**, 015001 (2001).

[49] E. Eichten, K. Lane, and M. Peskin, Phys. Rev. Lett. **50**, 811 (1983).

[50] K. Cheung, S. Godfrey, and J. L. Hewett, in *Proceedings of the 1996 DPF/DPB Summer Study On New Directions For High-Energy Physics* (Snowmass 96), D. G. Cassel, L. T. Gennari, R. H. Siemann, eds. (Stanford, CA, 1997) [hep-ph/9612257].

[51] T. L. Barklow, Int. J. Mod. Phys **A11**, 1579 (1996).

[52] A. Leike, Phys. Reports **317** (1999) 143; M. Cvetič, S. Godfrey, in "Electroweak Symmetry Breaking and Beyond the Standard Model", T. Barklow, S. Dawson, H. Haber, J. Siegrist eds., World Scientific 1995; S. Godfrey, Phys. Rev. **D51**, 1402 (1995); S. Godfrey, J. Hewett, and L. Price, in *Proceedings of the 1996 DPF/DPB Summer Study On New Directions For High-Energy Physics* (Snowmass 96), D. G. Cassel, L. T. Gennari, R. H. Siemann, eds. (Stanford, CA, 1997) [hep-ph/9704291]; T. Rizzo, *ibid.*, [hep-ph/9612440].

[53] S. Godfrey, P. Kalyniak, B. Kamal, A. Leike, Phys. Rev. **D61**, 113009 (2000).

[54] J. Hewett, in *Proceedings of the 1996 DPF/DPB Summer Study On New Directions For High-Energy Physics* (Snowmass 96), D. G. Cassel, L. T. Gennari, R. H. Siemann, eds. (Stanford, CA, 1997) [hep-ph/9704292].

[55] M. Doncheski, S. Godfrey, P. Kalyniak, B. Kamal, A. Leike, Phys. Rev. **D63**, 053005 (2001).

[56] S. Riemann, LC-TH-2001-007 and in *Proceedings of the 5th International Linear Collider Workshop* (LCSW2000).

[57] W. Buchmüller, R. Rückl and D. Wyler, Phys. Lett. **B191**, 442 (1987).

[58] A. F. Żarnecki, Eur. Phys. J. **C17**, 695 (2000).

[59] M. Heyssler, R. Rückl, and H. Spiesberger, in *International Workshop on Linear Colliders*, Sitges, Spain, 1999, hep-ph/9908319.

[60] M. A. Doncheski and S. Godfrey, Phys. Rev. **D49**, 6220 (1994); Phys. Rev. **D51**, 1040 (1995); Phys. Lett. **B393**, 355 (1997); J. L. Hewett and S. Pakvasa, Phys. Lett. **B227**, 178 (1989).

[61] J. L. Hewett and T. G. Rizzo, Phys. Rev. **D36**, 3367 (1987); J. Blümlein and R. Rückl, Phys, Lett. **B304**, 337 (1993); J. Hewett in *2nd International Workshop on Physics and Experimentation with e^+e^- Linear Colliders*, Waikoloa, HI, 1993, hep-ph/9308321.

[62] S. Abdullin and F. Charles, Phys. Lett. **B464**, 223 (1999).

[63] J. L. Hewett and T. G. Rizzo, Phys. Rev. **D56**, 5709 (1997).

[64] A. Djouadi, J. Ng, and T. G. Rizzo, in *Electroweak Symmetry Breaking and New Physics at the TeV Scale*, ed. T. Barklow *et al.*, (World Scientific, Singapore), 416 (1996).

[65] J. Maalampi, K. Mursula and M. Roos, Nucl. Phys. **207B**, 233 (1982).

[66] J. L. Hewett and T. G. Rizzo, Phys. Rep. **183**, 193 (1989).

[67] J. W. F. Valle, Nucl. Phys. Proc. Suppl. **11**, 119 (1989).

[68] P. Langacker and D. London, Phys. Rev. **D38**, 886 (1988). E. Nardi, E. Roulet and D. Tommasini, Nucl. Phys. **386B**, 239 (1992), Phys. Lett. **327B**, 319 (1994). F. M. L. Almeida Jr. *et al.*, Phys. Rev. **D62**, 075004 (2000).

[69] V. Barger, T. Han, and J. Ohnemus, Phys. Rev. **D37**, 1174 (1988); V. Barger and R. Phillips, *Collider Physics*, (New York, Addison Wesley, 1987).

[70] A. Djouadi, Z. Phys. **C63**, 317 (1994); G. Azuelos and A. Djouadi, Z. Phys. **C63**, 327 (1994).

[71] F. M. L. Almeida Jr. *et al.*, Phys. Rev. **D51**, 5990 (1995).

[72] F. M. L. Almeida Jr. *et al.*, Phys. Rev. **D63**, 075005 (2001).

[73] N. Arkani-Hamed, S. Dimopoulos, and G. Dvali, Phys. Lett. **B429**, 263 (1998), and Phys. Rev. **D59**, 086004 (1999); I. Antoniadis, N. Arkani-Hamed, S. Dimopoulos, and G. Dvali, Phys. Lett. **B436**, 257 (1998).

[74] L. Randall and R. Sundrum, Phys. Rev. Lett. **83**, 3370 (1999), and *ibid.*, 4690, (1999).

[75] I. Antoniadis, Phys. Lett. **B246**, 377 (1990); J. Lykken, Phys. Rev. **D54**, 3693 (1996); E. Witten, Nucl. Phys. **B471**, 135 (1996); P. Horava and E. Witten, Nucl. Phys. **B460**, 506 (1996), *ibid.*, **B475**, 94 (1996).

[76] N. Arkani-Hamed and M. Schmaltz, Phys. Rev. **D61**, 033005 (2000); N. Arkani-Hamed, Y. Grossman and M. Schmaltz, Phys. Rev. **D61**, 115004 (2000); E. A. Mirabelli and M. Schmaltz, Phys. Rev. **D61**, 113001 (2000); G. C. Branco, A. De Gouvea and M. N. Rebolo, hep-ph/0012289; T. G. Rizzo, hep-ph/0101278.

[77] H. Cheng, B. A. Dobrescu and C. T. Hill, Nucl. Phys. **B589**, 249 (2000) [hep-ph/9912343]; B. A. Dobrescu, Phys. Lett. **B461**, 99 (1999) [hep-ph/9812349].

[78] N. Arkani-Hamed, H. Cheng, B. A. Dobrescu and L. J. Hall, Phys. Rev. **D62**, 096006 (2000) [hep-ph/0006238].

[79] B. A. Dobrescu and E. Poppitz, hep-ph/0102010.

[80] C. D. Hoyle, U. Schmidt, B. R. Heckel, E. G. Adelberger, J. H. Gundlach, D. J. Kapner and H. E. Swanson, Phys. Rev. Lett. **86**, 1418 (2001) [hep-ph/0011014].

[81] G. F. Giudice, R. Rattazzi, and J. D. Wells, Nucl. Phys. **B544**, 3 (1999).

[82] S. Cullen and M. Perelstein, Phys. Rev. Lett. **83**, 268 (1999); L. Hall and D. Smith, Phys. Rev. **D60**, 085008 (1999); V. Barger, T. Han, C. Kao, and R. J. Zhang, Phys. Lett. **B461**, 34 (1999); C. Hanhart, D. R. Phillips, S. Reddy, and M. J. Savage nucl-th/0007016.

[83] See, for example, T. G. Rizzo and J. D. Wells, Phys. Rev. **D61**, 016007 (2000); P. Nath and M. Yamaguchi, Phys. Rev. **D60**, 116006 (1999); M. Masip and A. Pomarol, Phys. Rev. **D60**, 096005 (1999); W. J. Marciano, Phys. Rev. **D60**, 093006 (1999); L. Hall and C. Kolda, Phys. Lett. **B459**, 213 (1999); R. Casalbuoni, S. DeCurtis and D. Dominici, Phys. Lett. **B460**, 135 (1999); R. Casalbuoni, S. DeCurtis, D. Dominici and R. Gatto, Phys. Lett. **B462**, 48 (1999); A. Strumia, Phys. Lett. **B466**, 107 (1999); F. Cornet, M. Relano and J. Rico, Phys. Rev. **D61**, 037701 (2000); C. D. Carone, Phys. Rev. **D61**, 015008 (2000); A. Delgado, A. Pomarol and M. Quiros, JHEP **0001**, 030 (2000).

[84] T. Han, J. Lykken, and R. J. Zhang, Phys. Rev. **D59**, 105006 (1999) .

[85] E. A. Mirabelli, M. Perelstein, and M. Peskin, Phys. Rev. Lett. **82**, 2236 (1999); K. Cheung and W. Y. Keung Phys. Rev. **D60**, 112003 (1999).

[86] G.W. Wilson, LC-PHSM-2001-010; A. Vest, LC-TH-2000-058, http://www.desy.de/~lcnotes.

[87] M. Gataullin, talk presented at *36ᵗʰ Rencontres de Moriond on Electroweak Interactions and Unified Theories*, Les Arcs, France, 10-17 March 2001; G. Landsberg, *ibid.*, A. Schoning, *ibid.*, D. Bourilkov, hep-ex/0103039; B. Abbott *et al.*, (DØ Collaboration), Phys. Rev. Lett. **86**, 1156 (2001).

[88] L. Vacavant and I. Hinchliffe, SN-ATLAS-2001-005, to appear in J. Phys. G.

[89] J. L. Hewett Phys. Rev. Lett. **82**, 4765 (1999); T. G. Rizzo, Phys. Rev. **D59**, 115010 (1999).

[90] M. Bando, T. Kugo, T. Noguchi, and K. Yoshioka Phys. Rev. Lett. **83**, 3601 (1999); J. Hisano, and N. Okada Phys. Rev. **D61**, 106003 (2000).

[91] O. J. P. Eboli, T. Han, M. B. Magro, and P. C. Mercadante, Phys. Rev. **D61**, 094007 (2000).

[92] E. Dudas, J. Mourad, Nucl. Phys. **B575**, 3 (2000); E. Accomando, I. Antoniadis, K. Benakli, Nucl. Phys. **B579**, 3 (2000); S. Cullen, M. Perelstein, M. E. Peskin, Phys. Rev. **D62**, 055012 (2000).

[93] A. Miagkov, talk presented at *Workshop on Higgs and Supersymmetry*, Orsay, France, 11-22 March, 2001.

[94] T. G. Rizzo, Phys. Rev. **D60**, 115010 (1999); H. Davoudiasl, Phys. Rev. **D60**, 084022 (1999); Phys. Rev. **D61**, 044018 (2000).

[95] D. Sadri and J. L. Hewett, SLAC-PUB-8782 (2001).

[96] W. D. Goldberger and M. B. Wise Phys. Rev. Lett. **83**, 4922 (1999); O. DeWolfe, D. Z. Freedman, S. S. Gubser, and A. Karch, Phys. Rev. **D62**, 046008 (2000); M. A. Luty and R. Sundrum, Phys. Rev. **D62**, 035008 (2000).

[97] H. Davoudiasl, J. L. Hewett, and T. G. Rizzo, Phys. Rev. Lett. **84**, 2080 (2000).

[98] H. Davoudiasl, T. G. Rizzo, hep-ph/0104199.

[99] H. Davoudiasl, J. L. Hewett, and T. G. Rizzo, Phys. Rev. **D63**, 075004 (2001).

[100] B. C. Allanach, K. Odagiri, M. A. Parker, and B. R. Webber, JHEP **0009**, 019 (2000).

[101] H. Davoudiasl, J. L. Hewett, and T. G. Rizzo, Phys. Lett. **B473**, 43 (2000) and hep-ph/0006097; A. Pomarol, Phys. Lett. **B486**, 153 (2000); Y. Grossman and M. Neubert, Nucl. Phys. **B474**, 361 (2000); R. Kitano, Phys. Lett. **B481**, 39 (2000); S. Chang *et al.*, Phys. Rev. **D62**, 084025 (2000); T. Ghergetta and A. Pomarol, Nucl. Phys. **B586**, 141 (2000).

[102] It will be assumed in the discussion below that all of the SM gauge fields are in the bulk. See, for example, I. Antoniadis, C. Munoz and M. Quiros, Nucl. Phys. **B397**, 515 (1993); I. Antoniadis and K. Benalki, Phys. Lett. **B326**, 69 (1994), and Int. J. Mod. Phys. **A15**, 4237 (2000); I. Antoniadis, K. Benalki and M. Quiros, Phys. Lett. **B331**, 313 (1994); K. Benalki, Phys. Lett. **B386**, 106 (1996); T. G. Rizzo, Phys. Rev. **D61**, 055005 (2000).

[103] E. Tourneifer, talk presented at the 36th *Rencontres de Moriond on Electroweak Interactions and Unified Theories*, Les Arcs, France, 10-17 March 2001.

[104] G. Azuelos, and G. Polesello, in preparation.

[105] T. G. Rizzo, Phys. Rev. **D61**, 055005 (2000).

[106] Finite KK sums can also arise from other kinds of new physics; see for example, M. Bando, T. Kugo, T. Noguchi and K. Yoshioka, hep-ph/9906549; I. Antoniadis, K. Benalki and M. Quiros, hep-ph/9905311.

[107] T.G. Rizzo, hep-ph/0101278.

[108] N. Arkani-Hamed, Y. Grossman, and M. Schmaltz, Phys. Rev. **D61**, 115004 (2000).

[109] T. Appelquist, H.-C. Cheng and B. A. Dobrescu, hep-ph/0012100; R. Barbieri, L. J. Hall and Y. Nomura, hep-ph/0011311.

[110] A. De Rujula, A. Donini, M. B. Gavela, S. Rigolin, Phys. Lett. **B482**, 195 (2000).

[111] S. Cullen, M. Perelstein, and M. E. Peskin Phys. Rev. **D62**, 055012 (2000).

[112] G. Veneziano, Nuovo Cim. **A57**, 190 (1968).

[113] For a review of non-commutative theories, see, N. Seiberg and E. Witten, JHEP **9909**, 032 (1999).

[114] S. M. Carroll *et al.*, hep-th/0105082.

[115] J. L. Hewett, F. J. Petriello, T. G. Rizzo, hep-ph/0010354.

[116] T. G. Rizzo, Phys. Rev. **D59**, 113004 (1999).